

Chemical Geology

Origin and evolution of the slab fluids since subduction inception in the Izu-Bonin-Mariana : A comparison with the southeast Mariana fore-arc rift --Manuscript Draft--

Manuscript Number:	CHEMGE13988R1
Article Type:	Research paper
Keywords:	Subduction inception, slab fluid, Izu-Bonin-Mariana, SEMFR, proto-arc crust, boninites, subduction zone
Corresponding Author:	Julia Ribeiro, PhD Guangzhou Institute of Geochemistry Guangzhou, CHINA
First Author:	Julia Ribeiro, PhD
Order of Authors:	Julia Ribeiro, PhD Christopher MacLeod Johan Lissenberg Jeff Ryan Colin Macpherson
Abstract:	<p>Subduction zones have played a central role in exchanging volatiles (H₂O, CO₂, S, halogens) between the different Earth's reservoirs throughout its history. Fluids that are released as the subducted plates dehydrate are major agents that transfer these volatiles inside the Earth; but the origins and the compositional evolution of the slab fluids as plates begin to sink are yet to be understood. To explore processes that take place during subduction infancy, here we examine the compositions of proto-arc magmas from the Izu-Bonin-Mariana (IBM) convergent margin that formed during subduction inception; and we compare these to a modern example of near-trench spreading in the southeast Mariana fore-arc rift (SEMFR). There is a temporal and spatial evolution in the slab fluid composition that is accompanied with a change in the fluid reservoirs, as subduction progresses. During the early stages of the subduction zone, dehydration of the serpentinized subducting mantle likely triggered dehydration and melting of the altered oceanic crust in the amphibolite facies to produce boninites. As the subduction zone matured, the volcanic arc front was displaced away from the trench. The arc magmas captured deeper slab fluids released from the subducted oceanic crust, the sediments and the underlying serpentinized mantle. Dehydration and melting of the subducted sediment became more prevalent with time and increasing slab depth (~100 km) to produce arc magmas. This compositional evolution was associated with a deepening of magma generation, which is likely accompanied with the progressive serpentinization of fore-arc mantle. Hence, fore-arc mantle serpentinization might have facilitated arc maturation and subduction stabilization throughout IBM history.</p>

1 **Origin and evolution of the slab fluids since subduction inception in the Izu-Bonin-**
2 **Mariana: A comparison with the southeast Mariana fore-arc rift**

3 Julia Ribeiro¹, Christopher MacLeod², Johan Lissenberg², Jeff Ryan³, Colin Macpherson⁴

4
5 ¹State Key Laboratory of Isotope Geochemistry, Guangzhou Institute of Geochemistry,
6 Chinese Academy of Sciences, Guangzhou 510640, China.

7 ² Department of Earth and Environmental Sciences, Cardiff University, Cardiff, Wales, CF10
8 3AT, UK.

9 ³ University of South Florida, School of Geosciences, Tempa, FL, USA.

10 ⁴ Department of Earth Science, Durham University, Durham, UK.

11
12 **Abstract**

13 Subduction zones have played a central role in exchanging volatiles (H₂O, CO₂, S, halogens)
14 between the different Earth's reservoirs throughout its history. Fluids that are released as the
15 subducted plates dehydrate are major agents that transfer these volatiles inside the Earth; but
16 the origins and the compositional evolution of the slab fluids as plates begin to sink are yet to
17 be understood. To explore processes that take place during subduction infancy, here we
18 examine the compositions of proto-arc magmas from the Izu-Bonin-Mariana (IBM) convergent
19 margin that formed during subduction inception; and we compare these to a modern example
20 of near-trench spreading in the southeast Mariana fore-arc rift (SEMFR). There is a temporal
21 and spatial evolution in the slab fluid composition that is accompanied with a change in the
22 fluid reservoirs, as subduction progresses. During the early stages of the subduction zone,
23 dehydration of the serpentinized subducting mantle likely triggered dehydration and melting
24 of the altered oceanic crust in the amphibolite facies to produce boninites. As the subduction
25 zone matured, the volcanic arc front was displaced away from the trench. The arc magmas
26 captured deeper slab fluids released from the subducted oceanic crust, the sediments and the

27 underlying serpentinized mantle. Dehydration and melting of the subducted sediment became
28 more prevalent with time and increasing slab depth (≥ 100 km) to produce arc magmas. This
29 compositional evolution was associated with a deepening of magma generation, which is likely
30 accompanied with the progressive serpentinization of fore-arc mantle. Hence, fore-arc mantle
31 serpentinization might have facilitated arc maturation and subduction stabilization throughout
32 the IBM history.

33

34 **1- Introduction**

35 Subduction zones have efficiently cycled volatiles (H_2O , S, Cl, F, CO_2) between the
36 Earth's interior and the hydrosphere - atmosphere over geological time. The varying fluxes of
37 volatiles released at subduction zones have regulated explosive volcanism, which, in return,
38 has modulated and Earth's climate and habitability for millions of years.

39

40 During subduction, the subducted sediments are believed to dehydrate first, at about ~ 50
41 to 100 km depths, releasing water-rich slab fluids enriched in volatiles (CO_2 , H_2O , S, Cl) and
42 in fluid-mobile elements (Cs, Rb, Ba, Pb, U). These water-rich slab fluids serpentinize the
43 relatively cool ($\sim 600^\circ C$) fore-arc mantle wedge at shallow slab depth (< 100 km depth)
44 (Hyndman and Peacock, 2003; Rüpke et al., 2004; Savov et al., 2007). Dehydration of
45 subducted altered oceanic crust and serpentinized mantle occur at greater depths, of $\sim 100 -$
46 200 km depths, to trigger magmatism beneath the volcanic arc front and the back-arc basin
47 (Elliott et al., 1997; Grove et al., 2006; Pearce et al., 2005; Rüpke et al., 2004). As subduction
48 proceeds, the slab-derived fluids become less water-rich; and they progressively transition
49 into solute-rich slab fluids derived from sediment melting (or sediment melts) with increasing
50 slab depth (≥ 100 km) (Johnson and Plank, 1999; Kessel et al., 2005; Manning, 2004).
51 Volatile liberation from the incoming plate is discontinuous to sub-arc depth (Muñoz-

52 Montecinos et al., 2021), and the slab's capacity to carry water and other volatiles diminishes
53 with increasing depth (Rüpke et al., 2004; Schmidt and Poli, 1998). Although our
54 understanding of the formation and role of slab fluids has improved significantly over the
55 past decades, questions still remain regarding their origins and temporal-spatial
56 compositional evolution as subduction begins and the slab sinks progressively deeper. We
57 can wonder if this long-standing model also holds during the early development of a
58 subduction zone and throughout its lifespan. Does the composition of the slab fluids evolve
59 over time? Are the fluids released from the same part of the subducting slab during
60 subduction maturation?

61
62 To address these questions, we compiled a dataset from the Izu-Bonin-Mariana (IBM)
63 proto-arc crust (i.e., fore-arc basalts and boninites), the infant arc, and the mature volcanic arc
64 to examine the temporal variations in the compositions and in the sources of slab fluids since
65 subduction inception. We further compare the IBM proto-arc magmas to those from the
66 Southeast Mariana fore-arc rift (SEMFR), which developed by near-trench spreading long
67 after subduction initiated, to place additional constraints onto the subduction processes that
68 occur relatively close (within ~ 90 km) to the trench. We find that the slab fluid
69 compositions evolved over the lifetime of IBM. This compositional evolution reveals a
70 change in the sources of the slab fluids, which is associated with the progressive migration of
71 the volcanic arc front and a deepening of magma generation.

72

73 **2- Geological background**

74 **2.1- Temporal evolution of the IBM convergent margin**

75 The Izu-Bonin-Mariana fore-arc crust has long been regarded as a typical example of
76 proto-arc crust that developed during subduction inception (Fig. 1A) (Ishizuka et al., 2006;
77 Reagan et al., 2010; Stern and Bloomer, 1992). The IBM subduction zone is associated with

78 the sinking of the Pacific plate underneath the Philippine Sea plate, which initiated about 52
79 Myr ago (Fig. 2). Rapid sinking of the nascent slab enabled spreading of the proto-arc
80 oceanic lithosphere in front of the trench (called hereafter near-trench spreading) (Ishizuka et
81 al., 2006; Reagan et al., 2010; Stern and Bloomer, 1992). Hence, the asthenospheric mantle
82 flowed into the mantle wedge (i.e., the future fore-arc) and melted right above the descending
83 plate, producing new oceanic crust in front of the trench (Fig. 1A) (Ishizuka et al., 2006;
84 Maunder et al., 2020; Reagan et al., 2010). Several types of magmas were produced over the
85 IBM lifetime, as the subduction zone evolved; and these include:

86

87 • *Tholeiitic proto-arc basalts* (also named fore-arc basalts or FABs in the literature, after
88 Reagan et al. (2010)) which represent the first magmas emplaced as the slab began
89 sinking. These formed by decompression melting of the proto-arc asthenosphere with
90 limited infiltration of slab fluids from 52 to 48 Myr (Maunder et al., 2020; Pearce et
91 al., 1984; Reagan et al., 2010; Stern and Bloomer, 1992). Proto-arc lithosphere
92 accreted by spreading in front of the trench (i.e., near-trench spreading) during
93 subduction inception (Coulthard et al., 2021; Ishizuka et al., 2006; Ishizuka et al.,
94 2011a; Reagan et al., 2017).

95

96 • *Low-silica boninites (LSB)* which formed shortly after the FABs by near-trench
97 spreading from 51 to 48 Myr (Coulthard et al., 2021; Ishizuka et al., 2006; Reagan et
98 al., 2010; Shervais et al., 2019). As the subducted slab began to dehydrate and melt,
99 the resulting slab-derived fluids infiltrated the residual, depleted proto-arc
100 asthenosphere to produce the LSB (Ishizuka et al., 2006; Pearce and Reagan, 2019;
101 Reagan et al., 2017).

102

103 • Seafloor spreading rapidly transitioned into fluid-assisted mantle melting due to the
104 increasing fluxing of the depleted asthenosphere by the slab fluids, which produced
105 *high-silica boninites (HSB)* from 50 to 45 Myr (Coulthard et al., 2021; Li et al., 2019;
106 Pearce and Reagan, 2019; Reagan et al., 2010; Reagan et al., 2017; Shervais et al.,
107 2021; Stern and Bloomer, 1992) (Fig. 1A). The progressive compositional evolution
108 from the FABs to the high-Si boninites further implies that near-trench spreading
109 continuously transitioned from decompression mantle melting to fluid-assisted mantle
110 melting within 5-10 Myr following subduction inception (Coulthard et al., 2021;
111 Ishizuka et al., 2006; Ishizuka et al., 2011a; Reagan et al., 2010; Shervais et al., 2021;
112 Stern and Bloomer, 1992). HSB developed as small volcanic cones only a few
113 kilometers from the trench. Some of these volcanoes have been preserved in the IBM
114 fore-arc (Bonin Island, now called Chichijima; Fig. 2) (Reagan et al., 2010; Reagan et
115 al., 2017). Boninites represent the onset of arc magmatism, as they are the first melts
116 that formed by fluid-assisted mantle melting (Ishizuka et al., 2011a; Pearce and
117 Reagan, 2019; Reagan et al., 2010).

118
119 • *Infant arc magmas* appeared shortly after the eruption of the high-Si boninites, i.e.
120 from 45 to 41 Myr (Ishizuka et al., 2020; Ishizuka et al., 2011b; Reagan et al., 2017).
121 These represent the youngest arc volcanoes, which rapidly form within 10 Myr of
122 subduction inception (Ishizuka et al., 2006; Ishizuka et al., 2011b; Kanayama et al.,
123 2012). Arc infancy is a transient and short-lived stage (that lasted ~ 5 Myr) during
124 which small submarine and subaerial volcanic cones rapidly developed and migrated
125 away from the trench, without consolidating magma generation (Ishizuka et al., 2011a;
126 Ishizuka et al., 2020; Ribeiro et al., 2019). Some of these early arc volcanoes are

127 preserved in the Bonin Islands (Fig. 2) (Ishizuka et al., 2006; Kanayama et al., 2012,
128 2014).

129

130 • *The mature volcanic arc* began to develop from ~ 40 - 42 Myr and remains active
131 (Baker et al., 2008; Ishizuka et al., 2011b; Stern et al., 2013a; Tamura et al., 2014;
132 Tamura et al., 2011). The volcanic arc front has stabilized at its current location at ~
133 150 km from the trench the past 40 Myr (Ishizuka et al., 2011b; Straub et al., 2010;
134 Straub et al., 2015), and it lies ~ 100 - 150 km depth above the slab surface (Stern et
135 al., 2003). Magma generation has consolidated over time through the formation of
136 dykes and sills. This continuous supply of melts underneath the mature arc promoted
137 crustal thickening and magma differentiation.

138

139 As the IBM subduction zone matured and stabilized into a long-lived convergent margin,
140 progressive serpentinitization of the fore-arc mantle was accompanied by the retreat of the
141 infant volcanic arc front until stabilization. Hence, the conditions for a mature subduction
142 zone were rapidly established in IBM (≤ 10 Myr) (Ishizuka et al., 2006; Ishizuka et al.,
143 2020; Ishizuka et al., 2011b; Ribeiro et al., 2019; Straub et al., 2010; Straub et al., 2015).

144

145 **2.2- The southern Mariana fore-arc rift (SEMFR)**

146 The southern Mariana intra-oceanic arc represents the southern end of the Izu-Bonin-
147 Mariana (IBM) convergent margin (Fig. 2). To the south, Eocene proto-arc crust, that formed
148 during subduction infancy (Reagan et al., 2010), has undergone recent extension (< 5 Myr) to
149 accommodate opening of the Mariana Trough (Martinez et al., 2000; Martinez et al., 2018).

150 As a result, the southeast Mariana fore-arc rifts (SEMFR) opened in front of the trench due to
151 large-scale and disorganized lithospheric stretching above the shallow part of the subducting

152 Pacific plate (< 100 km depth to the slab), long after subduction had initiated (Fig. 1B). Slab
153 dehydration probably enhanced magmatic activity, resulting in a 6-km-thick and
154 homogeneous basaltic crust in the Mariana fore-arc (Martinez et al., 2018; Ribeiro et al.,
155 2013b). To the northwest, the SEMFR progressively transitions into the Fina-Nagu volcanic
156 chain (FNVC), which represents a juvenile arc that initiated less than 5 Myr ago (Brounce et
157 al., 2016; Ribeiro et al., 2019; Stern et al., 2013b). Near-trench spreading aborted within ~2
158 Myr (Martinez et al., 2018; Ribeiro et al., 2013a); and the inflated spreading ridges collapsed
159 as soon as magmatic activity ceased, forming the actual fore-arc rifts.

160

161 The SEMFR is now floored with recently erupted basaltic pillow lavas and lava flows
162 within 80-90 km from the trench (Martinez et al., 2018; Ribeiro et al., 2013a). The basalts are
163 underlain by a gabbroic lower crust and by a mixture of harzburgitic and refertilized
164 lherzolitic mantle (Michibayashi et al., 2009; Ohara and Ishii, 1998; Ribeiro et al., 2013a).
165 Even though near-trench spreading in the southern Marianas occurred long after subduction
166 initiated, the formation of new seafloor above a shallow dehydrating slab may be analogous
167 to the processes that occur during subduction inception. Hence, examining the SEMFR
168 magmas can provide critical insights into the shallow and near-trench subduction processes,
169 which are rarely captured in modern subduction zones.

170

171 3- **Data compilation and filtering**

172 To place additional constraints upon the processes that developed during subduction
173 infancy, we compiled a dataset (n = 1132) that includes bulk rock analyses and *in-situ* micro-
174 analyses of glasses from the SE Mariana fore-arc rift (SEMFR), the Izu-Bonin-Mariana
175 proto-arc crust, and the Mariana arc and back-arc. Fresh glass shards and olivine-hosted melt
176 inclusions were selected whenever possible, as they may have retained their primitive melt

177 compositions more faithfully than their host rock. Additionally, glass shards and olivine-
178 hosted melt inclusions have experienced the least degassing, and so may provide additional
179 constraints onto the volatile contents of water-rich slab fluids.

180

181 Because magmas degas upon ascent or during eruption, so fresh glass shards and
182 olivine-hosted melt inclusions were filtered for minimally degassed volatile contents ($\text{CO}_2 > 50$
183 ppm and S > 500 ppm), as in Kelley et al. (2006). Samples were then screened for basaltic (SiO_2
184 ≤ 56 wt%) and boninitic compositions (i.e., as reported in the literature) with a total sum of
185 oxides equal to 100 ± 2 wt% to ensure freshness and filtering for highly fractionated magma
186 compositions, as some fractionating mineral phases (amphibole, ilmenite, biotite, ...) could
187 modify trace element ratios (Schiano, 2003). Boninites are not excluded of our database for
188 high silica content, as neither low- nor high-silica boninites crystallize the mineral phases
189 which could modify their incompatible element ratios (i.e., olivine, spinel, orthopyroxene)
190 (Pearce et al., 2005). This filtering ($n = 521$) allows us to minimize the effects of volatile
191 degassing, alteration, crustal assimilation and contamination to ensure that the composition of
192 the magmas is most representative of their sources. Our filtered dataset includes 20 olivine-
193 hosted melt inclusions and 13 basaltic glass shards from the SEMFR, 203 olivine-hosted melt
194 inclusions, 11 basaltic glass shards and 29 bulk rocks from the Mariana arc, 46 bulk rocks and
195 47 basaltic glass shards from the Mariana Trough, 72 glass shards from the IBM proto-arc
196 crust, and 75 bulk rocks from the infant arc.

197 The water content of the glasses was also compared to incompatible elements, such as
198 Rb, that are mobilized with the aqueous slab fluids but remain unaffected by volatile degassing.
199 Correlations between water, Rb, MgO and SiO_2 indicates that the filtered dataset (i) glasses
200 have probably lost little water by degassing (Fig. S1-S4); and (ii) the melt inclusions did not
201 experience diffusive re-equilibration with the host olivine (Gaetani et al., 2012) . This filtered

202 dataset was used to examine the composition of slab fluids. However, we also used the
203 complete dataset to examine major element composition of the magmas as well as their Pb-Sr
204 isotopic ratios, which are rarely measured on fresh glass shards.

205

206 Despite their freshness, glasses can still be prone to secondary alteration processes
207 after being emplaced onto the seafloor. They can also have captured hydrothermal brines
208 within the magma chamber or upon ascent (Kent et al., 1999). Elements of interest (Ba, Rb,
209 Th, H₂O, ...) were plotted against elements that are believed to remain immobile during
210 alteration processes (see supplementary Fig. S1-S4). Fractionation trends were mostly
211 preserved, indicating that magmas were little affected by alteration (Fig. S1-S4). Hence, their
212 composition can be used to reliably track the composition of the slab fluids that infiltrated
213 their mantle source. The complete and the filtered datasets are reported in Table S1. Details
214 and references can be found in the supplementary material.

215

216 **4- Magma composition**

217 **4.1- From the IBM proto-arc to the mature arc magmas**

218 The IBM FABs are characterized by low K₂O (< 1 wt%) and low water contents (H₂O =
219 0.75 ± 0.58 (1σ) wt%) (Fig. 3A). They are however slightly enriched in water compared with
220 mid-ocean ridge basalts (H₂O < 0.2 wt%) (Saal et al., 2002). The low-silica (LSB) and the
221 high-silica boninites (HSB) possess higher K₂O content (> 0.2 wt%) and higher water content
222 (H₂O = 3.68 ± 1.21 (1σ) wt%) than the FABs (Fig. 3A). They are characterized by low TiO₂
223 content (< 0.4 wt%) (Fig. 3B) compared with the Mariana arc magmas, which indicates
224 melting of a strongly depleted, residual mantle source (Pearce and Reagan, 2019; Reagan et
225 al., 2017). In the MgO vs. SiO₂ diagram of Pearce and Reagan (2019), the FABs, the LSB
226 and the HSB plot along distinct liquid lines of descent, demonstrating that they did not form

227 during the same melting event. From the FABs to the HSB, there is an increase in the SiO₂
228 and K₂O contents of the magmas over time (stages 1 to 3 in Fig. 3A).

229 The infant arc magmas are low-K to medium-K basalts to dacites (Fig. 3A). As the arc
230 reaches maturity, the magmas become more enriched in K₂O, so that the mature arc magmas
231 are medium-K basalts to dacites. The infant arc magmas thus contrast with the more mature
232 Mariana arc by having lower K₂O content (Fig. 3A). This increase in the K₂O content of the
233 magmas during subduction maturation reveals the progressive migration and deepening of the
234 magma generation with time. Indeed, K-rich phases within the subducted slab, such as
235 lawsonite and phengite, tend to breakdown at sub-arc depth, so that the near-trench magmas
236 that overly a shallower part of the slab (≤ 90 km depth), capture K-poor, water-rich slab
237 fluids. By contrast, the infiltration of K-rich, water-rich aqueous slab fluids into the sub-arc
238 mantle enriches the arc magmas in K (Hatherton and Dickinson, 1969; Kimura and Stern,
239 2008; Pearce and Robinson, 2010; Plank and Langmuir, 1993; Schmidt and Poli, 1998) (Fig.
240 4-5). The low K₂O content of the early IBM magmas is thus consistent with their formation
241 within $\sim 90 - 100$ km from the trench and above a shallow, nascent subducted slab. The
242 mature arc magmas formed instead at $\sim 150 - 200$ km from the trench, and they overlie a
243 deeper portion of the slab (~ 100 km depth).

244

245 **4.2- The SEMFR magmas**

246 The SEMFR magmas are low-K basalts (SiO₂ < 59 wt%, K₂O ≤ 1 wt%) (Fig. 3A), and
247 contain 1.84 ± 0.39 (1σ) wt% H₂O on average. In terms of SiO₂, K₂O, MgO and TiO₂
248 contents, the SEMFR basalts are similar to FABs. Their higher TiO₂ content (> 0.4 wt%)
249 compared with the boninites (Fig. 3B), reveal that they formed by melting of a relatively
250 undepleted mantle source, as also shown by their Nb/Yb ~ 1 (Fig. 4).

251 The SEMFR basalts host some olivine mantle xenocrysts (Fo₉₀₋₉₂), which can enclose
252 fresh melt inclusions. The melt inclusions occur as isolated pieces of melt that are fully
253 entrapped by their olivine host. The melt inclusions were perhaps entrapped at $\sim 22.0 \pm 6.6$
254 km depth during olivine growth (Ribeiro et al., 2015). The SEMFR olivine-hosted melt
255 inclusions are primitive basalts (MgO > 8 wt%, SiO₂ < 54 wt%) that possess low K₂O (< 1
256 wt%) and low TiO₂ (< 0.5 wt%) contents (Fig. 3). In the classification diagram of Pearce and
257 Reagan (2019), the olivine-hosted melt inclusions overlap the compositional field for the
258 LSB (Fig. 3). This suggests melting of a more depleted mantle source than that of their host
259 lavas, and is consistent with their lower Nb/Yb ratios (~ 0.1) (Fig. 4). Ribeiro et al. (2015)
260 suggested that the SEMFR olivine-hosted melt inclusions trapped melts that formed by
261 adiabatic decompression mantle of the refractory fore-arc asthenosphere, that was infiltrated
262 by the water-rich slab fluids released during shallow slab dehydration. They proposed that the
263 recent stretching of the Eocene fore-arc lithosphere in the southern Marianas (~ 5 Myr ago)
264 enabled the fore-arc asthenosphere to flow in and melt under highly hydrous conditions
265 within 90 km from the trench. Near-trench spreading allowed the SEMFR magmas to erupt in
266 Pliocene time, while they captured mantle olivine upon ascent.

267

268 **5- Compositional evolution of the slab fluids since subduction inception**

269 Slab dehydration and slab melting can be inferred using chemical proxies (e.g., Rb/Th,
270 Cs/Th, H₂O/Ce, Th/Nb, La/Sm, Hf/Sm and Zr/Sm), which represent a record of the water-
271 rich and solute-rich slab fluids that participate in mantle melting (Elliott et al., 1997; Johnson
272 and Plank, 1999; Manning, 2004; Pearce et al., 2005). Ratios of a fluid-mobile element (Ba,
273 Cs, Rb, H₂O, Th, La) over an incompatible element that is not mobilized with the fluids (Nb,
274 Yb, Sm, Ce), but migrate similarly during mantle melting, has the advantage to minimize for
275 fractionation and melting processes. Hence, elemental ratios can preserve a reliable signature

276 of the slab fluids (Kogiso et al., 1997; McCulloch and Gamble, 1991). Because Ba, Rb and
277 Cs are mobilised by both with the water-rich fluids and the sediment melts, Rb/Th, Cs/Th and
278 Ba/Th ratios will track the water-rich slab fluids (Fig. 4–5), as Th is mainly mobilized during
279 sediment melting (Johnson and Plank, 1999; Pearce et al., 2005). Similarly, H₂O/Ce has been
280 used as a marker of water-rich slab fluids, as Ce remains relatively immobile with the water-
281 rich slab fluid (Dixon et al., 2017; Dixon et al., 2002; Ruscitto et al., 2012). The Ba/Nb,
282 Rb/Nb and Cs/Nb ratios track instead the total subduction signal (i.e., water-rich fluid and
283 solute-rich fluid); while Th/Nb ratios track the solute-rich fluids released during sediment
284 melting (Elliott et al., 1997; Pearce et al., 2005).

285 Hf/Sm and Zr/Sm ratios have been proposed to track melting of the oceanic crust in
286 the amphibolite facies (Foley et al., 2002; Li et al., 2019; Pearce et al., 1992), so that high
287 Hf/Sm and Zr/Sm ratios would reflect the infiltration of slab-derived amphibolite melts into
288 the mantle source. La/Sm, by contrast, tracks solute-rich fluids released by melting of both
289 the sediments and the amphibolitized oceanic crust. Amphibole is the only mineral phase
290 that fractionates Hf and Zr from Sm (Foley et al., 2002; Pearce et al., 1992). The scarcity of
291 amphibole in mantle rocks from modern subduction zones cannot account for the
292 compositional variations in Hf/Sm and Zr/Sm observed in the magmas (Pearce et al., 1992).
293 As such, slab melting of altered oceanic crust in the amphibolite facies has been proposed as
294 a cause of these variations, which is consistent with the observations of amphibolite melting
295 in subducted slabs with a warm P-T path (Angiboust et al., 2017; Prigent et al., 2018). Below,
296 we examine the composition of slab fluid markers in magmatism spanning the history of the
297 IBM margin.

298

299 **5.1- Large fluxes of water-rich slab fluids released during subduction infancy**

300 The FABs possess a geochemical fingerprint in the markers of water-rich slab fluids that
301 is intermediate between mid-ocean ridge basalts (MORBs) and back-arc basin basalts
302 (BABBs) ($Ba/Th = 63.26 - 92.47$, $Rb/Th = 5.50 - 39.54$, $Cs/Th = 0.05 - 0.54$, $H_2O/Ce =$
303 $484.06 - 2798.09$; Table S1-4) (Fig. 4-5), indicating that a minor amount of slab fluid
304 infiltrated the asthenospheric mantle during the first stages of subduction inception in IBM
305 (Coulthard et al., 2021; Ishizuka et al., 2011b; Reagan et al., 2010; Reagan et al., 2017).
306 There is an increase in the markers of slab dehydration from the FABs to the boninites
307 ($Ba/Th = 133.01 - 913.18$, $Rb/Th = 30.41 - 219.32$, $Cs/Th = 0.53 - 4.79$ for the LSB glasses;
308 and $Ba/Th = 115.65 - 239.90$, $Rb/Th = 51.19 - 134.23$, $Cs/Th = 1.71-5.17$ for the HSB
309 glasses in Fig. 4-5; Table S1-4), that is associated with an increase in H_2O/Ce (Fig. 4A). The
310 boninites also possess higher H_2O/Ce ratios ($7522.55 - 21775.79$) compared with the modern
311 arc and the back-arc magmas. Although HSB have slightly higher markers of slab
312 dehydration than LSB, their compositional ranges generally overlap (Fig. 4-5, 7). The sharp
313 increase in the markers of slab dehydration (Rb/Th , Ba/Th , Cs/Th , Cs/Ba) from the FABs to
314 the low-silica boninites further implies that large fluxes of water-rich fluids were released
315 from the shallow part of the subducting slab (≤ 90 km slab depth) within ~ 1 Myr of
316 subduction inception.

317 The high Th/Nb and La/Sm (Fig. 4, 6) in the IBM HSB further indicate that the subducted
318 sediments began melting shortly after the subduction began. The high Hf/Sm and Zr/Sm in
319 the IBM boninites (Fig. 6) has been proposed to track melting of the altered oceanic crust in
320 the amphibolite facies, due to high temperatures on top of the nascent slab (Foley et al., 2002;
321 Li et al., 2019; Pearce et al., 1992). Slab melting increases from the LSB to the HSB, as
322 shown by the higher Hf/Sm and Zr/Sm ratios in the HSB (Fig. 6). Such high temperatures
323 were perhaps caused by a return of asthenospheric mantle flow (Pearce and Robinson, 2010;
324 Reagan et al., 2010), triggered by the sinking of the nascent subducted plate. Slab melting in

325 the amphibolite facies during the early stages of IBM reveals the warm thermal structure of
326 the Pacific plate as it began sinking (Agard et al., 2020; Li et al., 2019; Prigent et al., 2018).
327 As subduction matures, its slab thermal structure progressively cools over time (Holt and
328 Condit, 2021).

329

330 **5.2- Less water-rich slab fluids and more sediment melts released beneath the** 331 **Mariana arc**

332 The infant arc basalts possess an intermediate composition between arc and back-arc
333 magmas in slab fluid proxies ($Ba/Th = 57.93 - 299.23$, $Rb/Th = 9.29 - 34.43$, $Th/Nb = 0.08 -$
334 0.87 ; Table S1-4) (light green compositional field Fig. 4) (Ribeiro et al., 2019). Their
335 composition in these slab-fluid markers is generally much lower than that observed in the
336 LSB and HSB (Fig. 4). During arc infancy, the slab fluids released from the slab at $\sim 90 - 100$
337 km depth progressively become less enriched in water and in sediment melt.

338 Mature arc basalts possess, instead, higher values for proxies of sediment melt ($Th/Nb =$
339 $0.18 - 1.17$) and water-rich fluids ($Ba/Th = 138.18 - 1141.18$, $Rb/Th = 6.86 - 33.04$, $Cs/Th =$
340 $0.23 - 1.23$, $H_2O/Ce = 1727.82 - 9828.55$; Table S1-5) than the infant arc magmas (Fig. 4-5).
341 The slab fluids released at sub-arc depths (≥ 100 km depth) beneath the mature volcanic arc
342 progressively became more aqueous and solute-rich, as compared to the fluids released
343 beneath the infant arc. However, these deeper slab fluids generally remained much less
344 aqueous than the shallow slab fluids released during subduction infancy (i.e., during boninitic
345 magmatism). Thus, there is a rapid decrease in the water-rich and solute-rich slab fluids from
346 the HSB to the infant arc magmas that occurred within 5 Myr of subduction inception (Fig. 6-
347 7). As the volcanic arc began to develop, the slab capacity to transport water, Rb and Cs to
348 depth diminished (Kessel et al., 2005; Manning, 2004; Schmidt and Poli, 1998); while
349 sediment melting became more prevalent at sub-arc depth (Fig. 4B).

350

351 **5.3- Slab fluid composition released beneath the SEMFR**

352 The SEMFR magmas possess lower Hf/Sm and Zr/Sm ratios (Fig. 6) than the
353 boninites, which suggests a cooler thermal structure on the mature subducted slab. Unlike the
354 nascent slab, the Pacific slab subducting underneath the Southern Marianas did not permit
355 melting of the oceanic crust in the amphibolite facies. The SEMFR basalts are however
356 strongly enriched in markers of slab dehydration ($Ba/Th = 93.86 - 798.36$, $Rb/Th = 9.51 -$
357 139.75 , $Cs/Th = 0.22 - 17.79$, $H_2O/Ce = 1799.06 - 18935.56$) (Fig. 4-5) compared to the
358 Mariana arc magmas ($Rb/Th \leq 68$, $Cs/Th \leq 4$, $H_2O/Ce \leq 9829$). The SEMFR basalts and
359 associated olivine-hosted melt inclusions display similar enrichments in markers of water-
360 rich slab fluids to those observed in the IBM boninites (Fig. 4-5). These results support the
361 notion that the shallow part of the downgoing plate could extensively dehydrate within ~ 90
362 km from the trench (≤ 90 km depths to the slab) in cold subduction zones (Angiboust and
363 Agard, 2010; Penniston-Dorland et al., 2015; Philippot, 1993; Ribeiro, 2022; Ribeiro et al.,
364 2015). Shallow slab dehydration seems to be accompanied by a decoupling between Ba from
365 Rb and Cs (as emphasized by the high Cs/Ba ratios of the SEMFR magmas and boninites in
366 Fig. 4C), which may reveal differential partitioning into water-rich slab fluids with increasing
367 slab depth (Bebout et al., 2007).

368

369 **6- Origin of the slab fluids released in IBM since subduction inception**

370 Pb-Sr radiogenic isotopes are commonly used to track the host reservoirs of the slab
371 fluids in subduction zone magmas, as Pb and Sr are both mobilized with sediment melts and
372 water-rich slab fluids (Kessel et al., 2005). Plotting markers of slab dehydration (Ba/Th) and
373 sediment melting (Th/Nb) against Pb-Sr radiogenic isotopes can thus place additional
374 constraints on how the sources of the slab fluids have varied throughout the lifetime of IBM

375 (Fig. 7-9). We also performed mixing calculations to assess the origin of the slab fluids and
376 quantify the contribution of the host reservoirs (i.e., subducted serpentized mantle, altered
377 oceanic crust and sediments). Details about our mixing equations and end-member
378 composition can be found in the supplementary material and in Table S2.

379

380 **6.1- Sources of the water-rich slab fluids released at shallow slab depth (≤ 90 km)**

381 Although subducted sediments are predicted to dehydrate first at shallow slab depths
382 (≤ 90 km depths) (Rüpke et al., 2004; Schmidt and Poli, 1998), the composition of the water-
383 rich slab fluids released from the sediments subducting underneath IBM may not account for
384 the compositional variations observed in the IBM boninites (both LSB and HSB) and the
385 SEMFR magmas. Indeed, the Ba, Cs, Rb do not seem to strongly partition into the water-rich
386 fluids released during sediment dehydration (Johnson and Plank, 1999). Hence, the inferred
387 compositions of sediment-derived, water-rich fluids possess much lower markers of slab
388 dehydration ($Rb/Th < 5$, $Ba/Th \leq 100$, $Cs/Th < 1$; see supplementary material and Table S2)
389 than those observed in the boninites and SEMFR magmas ($Ba/Th = 20.7 - 100.0$, $Rb/Th = 1.7$
390 $- 12.4$, $Cs/Th = 0.15 - 0.39$, $^{206}Pb/^{204}Pb = 19.03$) (Fig. 4-5, 8-10). For instance, the inferred
391 composition in Rb/Th and La/Sm of the sediment-derived, water-rich fluids cannot explain
392 the compositional variations observed in the SEMFR magmas and IBM boninites (Fig. 4C).
393 Retention of volatiles (H, C, N, S), alkalis (Rb, Cs) and other fluid-mobile elements (e.g., As,
394 Sb) in the subducted sediments beyond ~ 40 km depth has also been observed in
395 metasedimentary rocks from the Franciscan complex and the Western Baja Terrane (Bebout
396 et al., 2007; Sadofsky and Bebout, 2003). Such petrographic observations concur with the
397 notion that the subducted sediments would retain most of their intra-slab, water-rich fluids to
398 sub-arc depths to mainly contribute to the generation of arc magmas (Plank and Langmuir,
399 1993).

400

401 By contrast, Cs, Rb and Ba are easily partitioned into the water-rich fluids released
402 during dehydration of the underlying serpentinized mantle and the altered oceanic crust from
403 the subducting plate (Kessel et al., 2005; Scambelluri et al., 2001), so that their aqueous
404 fluids would have elevated Ba/Th, Cs/Th and Rb/Th ratios (Fig. 4-5, 8-10 and supplementary
405 material). Their dehydration could account for the compositional variations observed in the
406 IBM boninites, SEMFR basalts and associated olivine-hosted melt inclusions (Fig. 4-5).
407 Petrographic observations of cold subducting slabs (e.g., Western Alps and Zagros) and
408 modeled thermal structure of nascent slabs also suggest that the subducted oceanic crust and
409 the underlying serpentinized mantle are the main sources of water-rich slab fluids released at
410 shallow depths (≤ 90 km) (Angiboust et al., 2012; Holt and Condit, 2021; Muñoz-
411 Montecinos et al., 2021). They would release large fluxes of water-rich slab fluids beneath
412 the fore-arc as pulses from $\sim 50 - 80$ km the trench (Holt and Condit, 2021) within 2 to 5
413 Myr of subduction inception, as evidenced by the elevated markers of slab dehydration in the
414 boninites (Fig. 6).

415

416 **6.2- A temporal evolution in the fluid reservoirs throughout the lifetime of IBM**

417 The composition of the IBM magmas suggests a temporal change in the slab fluids
418 compositions that was associated with a change in their host reservoirs and increasing slab
419 depth (Fig. 6-10). This temporal evolution in magma composition, as highlighted in the
420 figures (Fig. 3, 6-10) by white numbers in black circles, is described as follows:

421

422 1- Formation of the FABs by near-trench spreading from 48 to 52 Myr (Ishizuka
423 et al., 2006; Reagan et al., 2019; Reagan et al., 2017). Limited slab fluids infiltrated
424 the relatively fertile asthenospheric mantle, which has a depleted MORB-like mantle

425 (DMM) composition (Fig. 4-6, 8-10). The low values of slab-fluid proxies suggest
426 that the nascent subducted Pacific slab dehydrated relatively little during subduction
427 inception (Coulthard et al., 2021; Reagan et al., 2019; Reagan et al., 2010).

428

429 2- Formation of the LSB by near-trench spreading from 48 to 50 Myr (Coulthard
430 et al., 2021; Reagan et al., 2019; Reagan et al., 2010). Water-rich and solute-rich slab
431 fluids progressively infiltrated the asthenospheric mantle residual to FAB melting, to
432 produce the LSB (Ishizuka et al., 2006; Reagan et al., 2019; Reagan et al., 2017). The
433 LSB marks the transition from adiabatic decompression melting to fluid-assisted
434 mantle melting (Coulthard et al., 2021; Reagan et al., 2019; Reagan et al., 2017;
435 Shervais et al., 2019). The $^{86}\text{Sr}/^{87}\text{Sr}$ isotopic composition of the LSB ($^{86}\text{Sr}/^{87}\text{Sr} <$
436 0.704) is lower than that of the HSB ($^{86}\text{Sr}/^{87}\text{Sr} > 0.704$), and is best explained by the
437 infiltration of water-rich fluids released from dehydrating of subducted crust and
438 serpentinized mantle into their mantle source (Fig. 8B). $^{208}\text{Pb}/^{204}\text{Pb}$ vs. $^{206}\text{Pb}/^{204}\text{Pb}$
439 variations (Fig. 10A) further suggest that there is a negligible contribution from the
440 subducted sediments in the LSB, and that altered oceanic crust dominates the
441 composition of the first fluids released from the nascent slab (Li et al., 2019). Our
442 mixing calculations suggest that the water-rich fluids released during the early stages
443 of IBM mainly come from dehydrating 50 – 100 % of the altered oceanic crust, and 0
444 - 50% of the serpentinized mantle. Up to 85 % of this water-rich slab fluid infiltrated
445 residual proto-arc mantle to produce the LSB (Fig. 8, 10). Deserpentinization of the
446 subducted mantle likely triggered dehydration and melting of the altered oceanic crust
447 in the amphibolite facies at shallow slab depth (< 100 km depth) (Fig. 6). The absence
448 of sediment fingerprint in the Pb isotopic composition of the LSB suggests that the

449 sediments were not subducted; and they were instead accreted or relatively limited
450 during the early stages of IBM (Li et al., 2019).

451

452 3- Formation of the HSB by fluid-assisted melting of the proto-arc mantle,
453 residual from LSB melting, from 45 to 50 Myr (Ishizuka et al., 2006; Reagan et al.,
454 2017). In contrast to the LSB, the Sr isotopic composition of the altered oceanic crust
455 cannot account for the Sr isotopic composition of the HSB, as the isotopic
456 composition of the oceanic crust in $^{87}\text{Sr}/^{86}\text{Sr}$ (0.7045) is too low (Fig. 8B). Instead,
457 the HSB are best explained by the infiltration of a water-rich fluid that was released
458 from dehydrating at least 50% subducted serpentized mantle and up to ~50%
459 sediments. Up to 60% of this composite fluid was captured by the HSB. These results
460 further suggest that the sediments began to be subducted within 2 – 3 Myr of
461 subduction inception. The Pb isotopic composition of the HSB (Fig. 8A, 10A-B) also
462 requires the involvement of a fluid from the altered oceanic crust, either as a water-
463 rich slab fluid or a solute-rich fluid. Variations in $^{206}\text{Pb}/^{204}\text{Pb}$ vs. Ba/Th (Fig. 8A)
464 further suggests that at least 50% altered oceanic crust and less than 50%
465 serpentized mantle is required to account for the compositional variations observed
466 in the HSB. Hence, the composition of the HSB is best explained by the infiltration of
467 water-rich slab fluids that were released from dehydrating altered oceanic crust (50 -
468 100%), the subducted serpentized mantle ($\leq 50\%$) and the subducted sediments (\leq
469 50%). Up to 60 to 85% of this water-rich slab fluid was captured by the HSB (Fig. 8,
470 10).

471 The solute-rich fluids captured by the HSB come from melting the oceanic
472 crust in the amphibolite facies (Fig. 6) (Li et al., 2019) and the subducted sediments
473 (Fig. 8C). Up to 35% of sediment melt infiltrated the proto-arc mantle. The

474 compositional variations in Th/Nb vs. $^{206}\text{Pb}/^{204}\text{Pb}$ of the HSB requires, however, an
475 end-member with high Th/Nb ratio ($\sim 1-3$) and lower Pb isotopic composition
476 ($^{206}\text{Pb}/^{204}\text{Pb} \sim 18.5$) than the Pacific sediments drilled at ODP Leg 129, Site 800 (Fig.
477 8C) (Plank and Langmuir, 1998). Such observations imply that the composition of
478 the Pacific sediments that subducted underneath IBM ~ 50 Myr ago might have been
479 much less radiogenic than are the sediments of ODP Site 800. Melting of the
480 subducted sediments triggered by dehydration of the subducted mantle offers a simple
481 alternative to that scenario. The resulting slab fluids would have had a Pb isotopic
482 composition (~ 18.5) intermediate between that of the sediment and the serpentinized
483 mantle.

484 Deserpentinization of the subducted mantle at shallow slab depths (< 100 km)
485 likely triggered dehydration and melting of the altered oceanic crust and the
486 subducted sediments, which facilitated melting of the residual, proto-arc mantle.
487 Hence, the sediments are progressively incorporated into the subducted slab through
488 time, as a *mélange* zone overlying the slab interface (Bebout, 2007; Cloos and
489 Shreve, 1988; Marschall and Schumacher, 2012) within $\sim 1-2$ Myr after subduction
490 inception (Li et al., 2019). Magma composition suggests that the sediment
491 contribution increased from the LSB to the HSB; while the contribution of the altered
492 oceanic crust decreased over time. The decreasing capacity in dehydrating the
493 subducted oceanic crust might indicate progressive slab eclogitisation at ~ 90 km
494 depths. This temporal change in the host reservoirs from the LSB to the HSB could
495 reflect a deepening of magma generation. The higher K_2O content of the HSB, as
496 compared to FABs and LSB (Fig. 3A), suggests that the HSB overlaid a deeper
497 portion of the subducted slab. Deepening of magma generation in the HSB could be

498 associated to a slab rollback and/or to a retreat of the melting front (Fig. 11) (Ishizuka
499 et al., 2006; Reagan et al., 2019; Reagan et al., 2010; Stern and Bloomer, 1992).

500

501 4- The infant arc began to develop at ~ 41 to 45 Myr, forming small trails of
502 subaerial and submarine volcanic cones within 90 km from the trench (Ishizuka et al.,
503 2011a; Kanayama et al., 2012, 2014). Infant arc magmas formed by melting of a
504 relatively fertile asthenosphere ($\text{Nb/Yb} \sim 1$ and $\text{TiO}_2 > 0.4$) that was infiltrated by
505 water-rich slab fluids and solute-rich melts. The sub-arc mantle was likely
506 replenished by the inflow of fresh asthenosphere. Variations in Ba/Th , $^{206}\text{Pb}/^{204}\text{Pb}$ and
507 $^{86}\text{Sr}/^{87}\text{Sr}$ suggest that the infant arc magmas captured the water-rich slab fluids
508 released from dehydrating 0-50% subducted mantle and 50-100% altered oceanic
509 crust; and 40-50% of this water-rich slab fluids infiltrated the sub-arc mantle (Fig.
510 8A). Variations in $^{208}\text{Pb}/^{204}\text{Pb}$ and $^{206}\text{Pb}/^{204}\text{Pb}$ further suggest that the subducted
511 sediments could also contribute to fingerprint the Pb isotopic composition of the
512 infant arc magmas, as depicted by a light green compositional field in Fig. 10A.
513 Hence, the subducted sediments could also dehydrate to some extent in the early arc,
514 as suggested by the variations in $^{86}\text{Sr}/^{87}\text{Sr}$ vs. Ba/Th (Fig. 8B). During that stage,
515 melting of the oceanic crust was negligible, so that the solute-rich fluids mostly
516 derived from sediment melting. The infant arc magmas captured the sediment melts
517 with a similar Pb isotopic composition to that observed in the HSB. 35% of sediment
518 melt was captured by the infant arc magmas (Fig. 8C).

519

520 5- The mature volcanic arc front began to develop ~ 40 – 42 Myr by fluid-assisted
521 melting of a relatively undepleted sub-arc mantle, forming larger and thicker-crust
522 volcanoes (Ishizuka et al., 2011b). The arc magmas captured the slab fluids released

523 from the deeper part of the subducted slab (~ 100 – 150 km depth), so that sediment
524 melting was more prevalent in the mature arc (Fig. 8C). The Pb-Sr isotopic
525 compositions of mature arc magmas suggest that the water-rich slab fluids were
526 released from dehydrating 50 - 100% altered oceanic crust, and 0 - 50% subducted
527 mantle, with a minor contribution from the sediments (Fig. 8A-B). However,
528 variations in Ba/Th and $^{206}\text{Pb}/^{204}\text{Pb}$ are best explained by mixing between 50% altered
529 oceanic crust and 50% subducted mantle (Fig. 8B). The solute-rich melts only came
530 from melting of the sediments (Fig. 8C). The mature arc magmas captured up to 40 %
531 of water-rich slab fluid and up to 70% of sediment melt. The contribution of the
532 solute-rich fluids released from the subducted sediments is much clearer in the mature
533 arc magmas (Fig. 4C, 8C) (Elliott, 2003; Johnson and Plank, 1999; Pearce et al.,
534 2005), implying that sediment melting become more prevalent at sub-arc depth.
535 Dehydration of the subducted serpentized mantle triggered dehydration and melting
536 of the overlying sediments, and dehydration of the altered oceanic crust (Klaver et al.,
537 2020).

538 The temporal change in slab-fluid reservoirs is likely associated with the
539 retreat of the volcanic arc front and a deepening of magma generation with time (Fig.
540 11). Arc migration is likely associated with serpentization and cooling of the fore-
541 arc mantle, which progressively displaces the depth of magma generation until it
542 stabilizes in its current location (i.e., ~ 100 – 150 km from the trench and ~ 100 km
543 depth to the slab) (Ribeiro et al., 2019). Hence, serpentization of the fore-arc mantle
544 could be essential in the development of a long-lived subduction zone (Agard et al.,
545 2020; Gerya et al., 2008; Hyndman and Peacock, 2003; Ribeiro and Lee, 2017;
546 Ribeiro et al., 2019). It would permit the formation of a subduction channel (Cloos
547 and Shreve, 1988), which could act as a lubricating layer on top of the subducted slab

548 that would facilitate deeper slab penetration and subduction stabilization (Agard et al.,
549 2020; Gerya et al., 2008).

550
551 **6.3- Comparison with the SEMFR magmas: Implications for the formation of the**
552 **IBM proto-arc crust**

553 The SEMFR magmas formed by near-trench spreading above a long-lived subduction
554 zone (Ribeiro et al., 2013a). The basalts possess similar chemical features to the FABs in
555 major element contents and in some of the trace element contents. However, unlike the
556 FABs, the SEMFR basalts captured greater extent of slab fluids. The SEMFR olivine-hosted
557 melt inclusions display similar features to the LSB in terms of major and trace element
558 contents, implying that they formed under similar (but not identical) petrogenetic conditions
559 (Fig. 3-4). The SEMFR basalts (bulk rock) display similar Pb-Sr isotopic composition to the
560 LSB (Fig. 9-10), which support the notion that they incorporated the slab fluids that were
561 released from the shallow part of the subducted slab (Ribeiro et al., 2013b). The water-rich
562 slab fluid was released from dehydrating at least 50% of the altered oceanic crust, less than
563 50% of subducted mantle (Fig. 9A-B). The SEMFR magmas captured 40% to 80% of this
564 water-rich slab fluids. Although sediments are subducted in the Southern Mariana Trench, the
565 SEMFR magmas possess similar Pb-Sr isotopic composition to that of the LSB (Fig. 8-10),
566 implying that the subducting sediments would retain most of their volatiles and alkalis to
567 release them at sub-arc depth. Hence, the subducting altered oceanic crust and the underlying
568 serpentinized mantle represent the main sources of water-rich slab fluids released beneath the
569 IBM fore-arc.

570 The strong enrichment in markers of water-rich slab fluids in the SEMFR glasses (Fig. 4-
571 6) further suggest that extensive slab dehydration could occur within ~ 90 km from the trench
572 both in mature (i.e., in the fore-arc) subduction zones (Ribeiro et al., 2015). Dehydration of
573 the subducted mantle and the altered oceanic crust likely dominates the water-rich slab fluids

574 released at shallow slab depths. Dehydration and melting of the subducted sediments become
575 more prevalent beneath the volcanic arc front (Johnson and Plank, 1999; Plank, 2005; Plank
576 and Langmuir, 1993, 1998). The sediments would thus retain most of their alkalis and some
577 of their volatiles to sub-arc depth to contribute to arc magma generation (Bebout et al., 2007;
578 Bebout et al., 1999; Busigny et al., 2003).

579 The fact that the SEMFR magmas display similar geochemical fingerprint to the IBM
580 proto-arc magmas further indicates that, despite having developed above a long-lived
581 subduction zone, the SEMFR can place important new constraints onto the processes that
582 occurred at the onset of a subduction zone. This is particularly important because there are a
583 few modern analogs to subduction infancy. These similarities further suggest that the IBM
584 proto-arc crust formed within 90 km from the trench and overlain a nascent slab at ≤ 90 km
585 depth or less. Such findings are consistent with the current location of the proto-arc crust that
586 has been preserved in the Bonin Island (Fig. 2) (Kanayama et al., 2012, 2014).

587

588 **7- Conclusions**

589 The composition slab-derived water-rich and solute-rich fluids evolved over the
590 lifetime of IBM (~ 52 Myr ago), reflecting a change in the sources of these fluids with time.
591 Markers of high slab dehydration (e.g., elevated Ba/Th, Rb/Th, Cs/Th, H₂O/Ce) recorded in
592 the IBM boninites indicate that large fluxes of water-rich slab fluids were mainly released
593 from dehydrating the subducted serpentinized mantle and from the altered oceanic crust
594 within 90 km from trench (≤ 90 km slab depth). As the subduction evolves, less water-rich
595 slab fluids are released from dehydrating the subducted serpentinized mantle and the altered
596 oceanic crust to sub-arc depths. The contribution from sediments, as water-rich and solute-
597 rich fluids, initiated later and hence deeper, suggesting that the sediments overlying the
598 Pacific plate were not subducted until ~ 50 Myr.

599 Changes in slab fluid compositions and in their sources reveal retreat of the volcanic
600 arc front, so that mature arc magmas captured slab fluids that are released from a deeper part
601 of the slab where sediment melting can occur. Therefore, mature arc magmas formed deeper
602 and they captured less water-rich slab fluids, compared to the shallow slab fluids released
603 during subduction infancy. Arc retreat and subduction stabilization in IBM were likely
604 modulated by the growth of the serpentinized fore-arc mantle, which could, therefore play a
605 key role in long-lived oceanic subduction zones. However, there is not a single scenario of
606 magma petrogenesis. Magma compositions depend upon the tectonic conditions, the thermal
607 structure of the subducted plate, and the mantle flow regime that prevail during subduction
608 evolution.

609

610 **Acknowledgements**

611 JR thanks Robert Stern (UTD), Julian Pearce (Cardiff University), Mark Reagan (Iowa
612 University), Jim Gill (University of California in Santa Cruz), Adam Kent (Oregon State
613 University), Susanne Straub (LDEO), Osamu Ishizuka and Yoshihiko Tamura (both at
614 JAMSTEC) for discussions that have inspired this manuscript over the past few years. Two
615 anonymous reviewers and Catherine Chauvel, the editor, are thanked for insightful
616 comments. JR acknowledge a PIFI fellowship n° 2020VCB000.

617

618 **References**

619 Agard, P., Prigent, C., Soret, M., Dubacq, B., Guillot, S., and Deldicque, D., 2020,
620 Slabification: Mechanisms controlling subduction development and viscous coupling:
621 Earth-Science Reviews, v. 208, p. 103259.
622 Angiboust, S., and Agard, P., 2010, Initial water budget: The key to detaching large volumes
623 of eclogitized oceanic crust along the subduction channel?: Lithos, v. 120, no. 3, p.
624 453-474.
625 Angiboust, S., Hyppolito, T., Glodny, J., Cambeses, A., Garcia-Casco, A., Calderón, M., and
626 Juliani, C., 2017, Hot subduction in the middle Jurassic and partial melting of oceanic
627 crust in Chilean Patagonia: Gondwana Research, v. 42, p. 104-125.

628 Angiboust, S., Wolf, S., Burov, E., Agard, P., and Yamato, P., 2012, Effect of fluid circulation
629 on subduction interface tectonic processes: Insights from thermo-mechanical
630 numerical modelling: *Earth and Planetary Science Letters*, v. 357-358, p. 238-248.

631 Baker, E. T., Embley, R. W., Walker, S. L., Resing, J. A., Lupton, J. E., Nakamura, K.-i., de
632 Ronde, C. E. J., and Massoth, G. J., 2008, Hydrothermal activity and volcano
633 distribution along the Mariana arc: *Journal of Geophysical Research*, v. 113, no. B8,
634 p. B08S09, DOI: 10.1029/2005GC000948.

635 Bebout, G. E., 2007, Metamorphic chemical geodynamics of subduction zones: *Earth and*
636 *Planetary Science Letters*, v. 260, no. 3–4, p. 373-393.

637 Bebout, G. E., Bebout, A. E., and Graham, C. M., 2007, Cycling of B, Li, and LILE (K, Cs, Rb, Ba,
638 Sr) into subduction zones: SIMS evidence from micas in high-P/T metasedimentary
639 rocks: *Chemical Geology*, v. 239, no. 3, p. 284-304.

640 Bebout, G. E., Ryan, J. G., Leeman, W. P., and Bebout, A. E., 1999, Fractionation of trace
641 elements by subduction-zone metamorphism — effect of convergent-margin
642 thermal evolution: *Earth and Planetary Science Letters*, v. 171, no. 1, p. 63-81.

643 Brounce, M. N., Kelley, K. A., Stern, R. J., Martinez, F., and Cottrell, E., 2016, The Fina Nagu
644 Volcanic Complex: Unusual submarine arc volcanism in the rapidly deforming
645 southern Mariana margin: *Geochemistry Geophysics Geosystems*, v. 17, p. 4078–
646 4091, doi:4010.1002/2016GC006457.

647 Busigny, V., Cartigny, P., Philippot, P., Ader, M., and Javoy, M., 2003, Massive recycling of
648 nitrogen and other fluid-mobile elements (K, Rb, Cs, H) in a cold slab environment:
649 evidence from HP to UHP oceanic metasediments of the Schistes Lustrés nappe
650 (western Alps, Europe): *Earth and Planetary Science Letters*, v. 215, no. 1, p. 27-42.

651 Cloos, M., and Shreve, R. L., 1988, Subduction-channel model of prism accretion, melange
652 formation, sediment subduction, and subduction erosion at convergent plate
653 margins: 1. Background and description: pure and applied geophysics, v. 128, no. 3,
654 p. 455-500.

655 Coulthard, D. A. J., Reagan, M. K., Shimizu, K., Bindeman, I. N., Brounce, M., Almeev, R. R.,
656 Ryan, J. G., Chapman, T., Shervais, J., and Pearce, J. A., 2021, Magma source
657 evolution following subduction initiation: Evidence from the element concentrations,
658 stable isotope ratios, and water contents of volcanic glasses from the Bonin forearc
659 (IODP Expedition 352): *Geochemistry Geophysics Geosystems*, v. 22, p.
660 e2020GC009054, <https://doi.org/009010.001029/002020GC009054>.

661 Dixon, J. E., Bindeman, I. N., Kingsley, R. H., Simons, K. K., Le Roux, P. J., Hajewski, T. R.,
662 Swart, P., Langmuir, C. H., Ryan, J. G., Walowski, K. J., Wada, I., and Wallace, P. J.,
663 2017, Light Stable Isotopic Compositions of Enriched Mantle Sources: Resolving the
664 Dehydration Paradox: *Geochemistry, Geophysics, Geosystems*, v. 18, no. 11, p. 3801-
665 3839.

666 Dixon, J. E., Leist, L., Langmuir, C. H., and Schilling, J.-G., 2002, Recycled dehydrated
667 lithosphere observed in plume-influenced mid-ocean-ridge basalt: *Nature*, v. 420,
668 no. 6914, p. 385-389.

669 Elliott, T. R., 2003, Tracers of the slab, *in* Eiler, J., ed., *Inside the Subduction Factory*, Volume
670 138: Washington, DC, Geophysical Monograph Series, p. 23-45.

671 Elliott, T. R., Plank, T., Zindler, A., White, W., and Bourdon, B., 1997, Element transport from
672 slab to volcanic front at the Mariana arc: *Journal of Geophysical Research*, v. B102, p.
673 14991-15019.

674 Foley, S., Tiepolo, M., and Vannucci, R., 2002, Growth of early continental crust controlled
675 by melting of amphibolite in subduction zones: *Nature*, v. 417, no. 6891, p. 837-840.

676 Gaetani, G. A., O'Leary, J. A., Shimizu, N., Bucholz, C. E., and Newville, M., 2012, Rapid
677 reequilibration of H₂O and oxygen fugacity in olivine-hosted melt inclusions:
678 *Geology*, v. 40, no. 10, p. 915-918.

679 Gerya, T. V., Connolly, J. A. D., and Yuen, D. A., 2008, Why is terrestrial subduction one-
680 sided?: *Geology*, v. 36, no. 1, p. 43-46.

681 Grove, T. L., Chatterjee, N., Parman, S. W., and Médard, E., 2006, The influence of H₂O on
682 mantle wedge melting: *Earth and Planetary Science Letters*, v. 249, no. 1–2, p. 74-89.

683 Hatherton, T., and Dickinson, W. R., 1969, The relationship between andesitic volcanism and
684 seismicity in Indonesia, the Lesser Antilles, and other island arcs: *Journal of*
685 *Geophysical Research (1896-1977)*, v. 74, no. 22, p. 5301-5310.

686 Holt, A., and Condit, C. B., 2021, Slab temperature evolution over the lifetime of a
687 subduction zone: *Geochemistry, Geophysics, Geosystems*, v. 22, no. 6, p.
688 e2020GC009476, <https://doi.org/009410.001029/002020GC009476>.

689 Hyndman, R. D., and Peacock, S. M., 2003, Serpentinization of the forearc mantle: *Earth and*
690 *Planetary Science Letters*, v. 212, no. 3–4, p. 417-432.

691 Ishizuka, O., Kimura, J.-I., Li, Y. B., Stern, R. J., Reagan, M. K., Taylor, R. N., Ohara, Y.,
692 Bloomer, S. H., Ishii, T., Hargrove Iii, U. S., and Haraguchi, S., 2006, Early stages in the
693 evolution of Izu–Bonin arc volcanism: New age, chemical, and isotopic constraints:
694 *Earth and Planetary Science Letters*, v. 250, no. 1–2, p. 385-401.

695 Ishizuka, O., Tani, K., Reagan, M. K., Kanayama, K., Umino, S., Harigane, Y., Sakamoto, I.,
696 Miyajima, Y., Yuasa, M., and Dunkley, D. J., 2011a, The timescales of subduction
697 initiation and subsequent evolution of an oceanic island arc: *Earth and Planetary*
698 *Science Letters*, v. 306, no. 3, p. 229-240.

699 Ishizuka, O., Taylor, R. N., Umino, S., and Kanayama, K., 2020, Geochemical Evolution of Arc
700 and Slab Following Subduction Initiation: a Record from the Bonin Islands, Japan:
701 *Journal of Petrology*, v. 61, no. 5.

702 Ishizuka, O., Taylor, R. N., Yuasa, M., and Ohara, Y., 2011b, Making and breaking an island
703 arc: A new perspective from the Oligocene Kyushu - Palau arc, Philippine Sea:
704 *Geochemistry Geophysics Geosystems*, v. 12, no. 5.

705 Johnson, M. C., and Plank, T., 1999, Dehydration and melting experiments constrain the fate
706 of subducted sediments: *Geochemistry Geophysics Geosystems*, v. 1, p. 1007, DOI:
707 10.1029/1999GC000014.

708 Kanayama, K., Umino, S., and Ishizuka, O., 2012, Eocene volcanism during the incipient stage
709 of Izu–Ogasawara Arc: *Geology and petrology of the Mukojima Island Group, the*
710 *Ogasawara Islands: Island Arc*, v. 21, no. 4, p. 288-316.

711 -, 2014, Shallow submarine volcano group in the early stage of island arc development:
712 *Geology and petrology of small islands south off Hahajima main island, the*
713 *Ogasawara Islands: Journal of Asian Earth Sciences*, v. 85, p. 1-25.

714 Kelley, K. A., Plank, T., Ludden, J. N., and Staudigel, H., 2003, Composition of altered oceanic
715 crust at ODP Sites 801 and 1149: *Geochem. Geophys. Geosyst.*, v. 4, no. 6, p. 8910,
716 DOI: 8910.1029/2002GC000435.

717 Kent, A. J. R., Norman, M. D., Hutcheon, I. D., and Stolper, E. M., 1999, Assimilation of
718 seawater-derived components in an oceanic volcano: evidence from matrix glasses
719 and glass inclusions from Loihi seamount, Hawaii: *Chemical Geology*, v. 156, no. 1–4,
720 p. 299-319.

721 Kessel, R., Schmidt, M. W., Ulmer, P., and Pettke, T., 2005, Trace element signature of
722 subduction-zone fluids, melts and supercritical liquids at 120–180 km depth: *Nature*,
723 v. 437, p. 724-727.

724 Kimura, J.-I., and Stern, R. J., 2008, Neogene volcanism of the Japan island arc: The K-h
725 relationship revisited, *in* Spencer, J. E., and Tittley, S. R., eds., *Ores and orogenesis:*
726 *Circum-Pacific tectonics, geologic evolution, and ore deposits*, Volume 22: Arizona,
727 Arizona Geological Society Digest, p. 187-202.

728 Klaver, M., Lewis, J. F., Parkinson, I. J., Elburg, M. A., Vroon, P. Z., Kelley, K. A., and Elliott, T.
729 R., 2020, Sr isotopes in arcs revisited: tracking slab dehydration using $\delta^{88/86}\text{Sr}$ and
730 $^{87}\text{Sr}/^{86}\text{Sr}$ systematics of arc lavas: *Geochimica et Cosmochimica Acta*, v. 288, p. 101-
731 119.

732 Kogiso, T., Tatsumi, Y., and Nakano, S., 1997, Trace element transport during dehydration
733 processes in the subducted oceanic crust: 1. Experiments and implications for the
734 origin of ocean island basalts: *Earth and Planetary Science Letters*, v. 148, no. 1–2, p.
735 193-205.

736 Li, H. Y., Taylor, R. N., Prytulak, J., Kirchenbaur, M., Shervais, J. W., Ryan, J. G., Godard, M.,
737 Reagan, M. K., and Pearce, J. A., 2019, Radiogenic isotopes document the start of
738 subduction in the Western Pacific: *Earth and Planetary Science Letters*, v. 518, p.
739 197-210.

740 Manning, C. E., 2004, The chemistry of subduction-zone fluids: *Earth and Planetary Science*
741 *Letters*, v. 223, no. 1-2, p. 1-16.

742 Marschall, H. R., and Schumacher, J., 2012, Arc magmas sourced from mélange diapirs in
743 subduction zones: *Nature Geoscience*, v. 5, no. 12, p. 862-867.

744 Martinez, F., Fryer, P., and Becker, N., 2000, Geophysical characteristics of the southern
745 Mariana Trough, 11°50'N-13°40'N: *Journal of Geophysical Research*, v. 105, no. B7, p.
746 16,591-516,607.

747 Martinez, F., Stern, R. J., Kelley, K., Ohara, Y., Sleeper, J. D., Ribeiro, J., and Brounce, M.,
748 2018, Diffuse extension of the southern Mariana margin: implications for subduction
749 zone infancy and plate tectonics: *Journal of Geophysical Research*, v. 123, p. 892–
750 916, <https://doi.org/810.1002/2017JB014684>.

751 Maunder, B., Prytulak, J., Goes, S., and Reagan, M., 2020, Rapid subduction initiation and
752 magmatism in the Western Pacific driven by internal vertical forces: *Nature*
753 *Communications*, v. 11, no. 1, p. 1874.

754 McCulloch, M. T., and Gamble, J. A., 1991, Geochemical and geodynamical constraints on
755 subduction zone magmatism: *Earth and Planetary Science Letters*, v. 102, no. 3–4, p.
756 358-374.

757 Michibayashi, K., Ohara, Y., Stern, R. J., Fryer, P., Kimura, J.-I., Tasaka, M., Harigane, Y., and
758 Ishii, T., 2009, Peridotites from a ductile shear zone within back-arc lithospheric
759 mantle, southern Mariana Trench: Results of a Shinkai 6500 dive: *Geochemistry*
760 *Geophysics Geosystems*, v. 10, no. 5, p. Q05X06, DOI: 10.1029/2008GC002197.

761 Muñoz-Montecinos, J., Angiboust, S., Garcia-Casco, A., Glodny, J., and Bebout, G. E., 2021,
762 Episodic hydrofracturing and large-scale flushing along deep subduction interfaces:
763 Implications for fluid transfer and carbon recycling (Zagros Orogen, southeastern
764 Iran): *Chemical Geology*, v. 571, p. 120173.

765 Ohara, Y., and Ishii, T., 1998, Peridotites from the southern Mariana forearc: Heterogeneous
766 fluid supply in mantle wedge: *Island Arc*, v. 7, no. 3, p. 541-558.

767 Pearce, J. A., Lippard, S. J., and Roberts, S., 1984, Characteristics and tectonic significance of
768 supra-subduction zone ophiolites: Geological Society, London, Special Publications,
769 v. 16, no. 1, p. 77-94.

770 Pearce, J. A., and Reagan, M. K., 2019, Identification, classification, and interpretation of
771 boninites from Anthropocene to Eoarchean using Si-Mg-Ti systematics: Geological
772 Society of America Bulletin, v. 15, no. 4, p. 1008-1037,
773 <https://doi.org/10.1130/GES01661.01661>.

774 Pearce, J. A., and Robinson, P. T., 2010, The Troodos ophiolitic complex probably formed in a
775 subduction initiation, slab edge setting: Gondwana Research, v. 18, no. 1, p. 60-81.

776 Pearce, J. A., Stern, R. J., Bloomer, S. H., and Fryer, P., 2005, Geochemical mapping of the
777 Mariana arc-basin system : Implications for the nature and distribution of subduction
778 components: Geochemistry Geophysics Geosystems, v. 6, no. 7, p. Q07006,
779 DOI:07010.01029/02004GC000895.

780 Pearce, J. A., Thirlwall, M. F., Ingram, G., Murton, B. J., Arculus, R. J., and Van der Laan, S. R.,
781 1992, Isotopic evidence for the origin of boninites and related rocks drilled in the Izu-
782 Bonin (Ogasawara) forearc, Leg 125, *in* Fryer, P., Pearce, J. A., and Stokking, L., et al.,
783 eds., Proceedings of the Ocean Drilling Program, Scientific Results 125, Volume 125:
784 Texas A&M University, Austin, Tx, IODP, p. 237-261,
785 <http://dx.doi.org/210.2973/odp.proc.sr.2125.2134.1992>.

786 Peccerillo, A., and Taylor, S. R., 1976, Geochemistry of Eocene calcalkaline volcanic rocks
787 from the Kastamonu Area, Northern Turkey: Contribution to Mineralogy and
788 Petrology, v. 58, p. 63-81.

789 Penniston-Dorland, S. C., Kohn, M. J., and Manning, C. E., 2015, The global range of
790 subduction zone thermal structures from exhumed blueschists and eclogites: Rocks
791 are hotter than models: Earth and Planetary Science Letters, v. 428, p. 243-254.

792 Philippot, P., 1993, Fluid-melt-rock interaction in mafic eclogites and coesite-bearing
793 metasediments: Constraints on volatile recycling during subduction: Chemical
794 Geology, v. 108, no. 1, p. 93-112.

795 Plank, T., 2005, Constraints from Thorium/Lanthanum on Sediment Recycling at Subduction
796 Zones and the Evolution of the Continents: Journal of petrology, v. 46, no. 5, p. 921-
797 944.

798 Plank, T., and Langmuir, C. H., 1993, Tracing trace elements from sediment input to volcanic
799 output at subduction zones: Nature, v. 362, no. 6422, p. 739-743.

800 -, 1998, The chemical composition of subducting sediment and its consequences for the
801 crust and mantle: Chemical Geology, v. 145, no. 3-4, p. 325-394.

802 Prigent, C., Guillot, S., Agard, P., Lemarchand, D., Soret, M., and Ulrich, M., 2018, Transfer of
803 subduction fluids into the deforming mantle wedge during nascent subduction:
804 Evidence from trace elements and boron isotopes (Semail ophiolite, Oman): Earth
805 and Planetary Science Letters, v. 484, p. 213-228.

806 Reagan, M. K., Heaton, D. E., Schmitz, M. D., Pearce, J. A., Shervais, J. W., and Koppers, A. A.
807 P., 2019, Forearc ages reveal extensive short-lived and rapid seafloor spreading
808 following subduction initiation: Earth and Planetary Science Letters, v. 506, p. 520-
809 529.

810 Reagan, M. K., Ishizuka, O., Stern, R. J., Kelley, K. A., Ohara, Y., Blichert-Toft, J., Bloomer, S.
811 H., Cash, J., Fryer, P., Hanan, B. B., Hickey-Vargas, R., Ishii, T., Kimura, J.-I., Peate, D.
812 W., Rowe, M. C., and Woods, M., 2010, Fore-arc basalts and subduction initiation in

813 the Izu-Bonin-Mariana system: *Geochemistry Geophysics Geosystems*, v. 11, no. 3, p.
814 Q03X12, DOI: 10.1029/2009GC002871.

815 Reagan, M. K., Pearce, J. A., Petronotis, K., Almeev, R. R., Avery, A. J., Carvallo, C., Chapman,
816 T., Christeson, G. L., Ferré, E. C., Godard, M., Heaton, D. E., Kirchenbaur, M., Kurz,
817 W., Kutterolf, S., Li, H., Li, Y., Michibayashi, K., Morgan, S., Nelson, W. R., Prytulak, J.,
818 Python, M., Robertson, A. H. F., Ryan, J. G., Sager, W. W., Sakuyama, T., Shervais, J.
819 W., Shimizu, K., and Whattam, S. A., 2017, Subduction initiation and ophiolite crust:
820 new insights from IODP drilling: *International Geology Review*, v. 59, no. 11, p. 1439-
821 1450.

822 Ribeiro, J., 2022, Slab dehydration beneath forearcs: Insights from the southern Mariana
823 and Matthew-Hunter rifts: *Geochemical Perspective Letters*, v. 20, p. 22–26, doi:
824 10.7185/geochemlet.2203.

825 Ribeiro, J., and Lee, C. T. A., 2017, An imbalance in the deep water cycle at subduction
826 zones: The potential importance of the fore-arc mantle: *Earth and Planetary Science*
827 *Letters*, v. 479, p. 298-309, <https://doi.org/210.1016/j.epsl.2017.1009.1018>.

828 Ribeiro, J., Stern, R. J., Martinez, F., Ishizuka, O., Merle, S. G., Kelley, K. A., Anthony, E. Y.,
829 Ren, M., Ohara, Y., Reagan, M., Girard, G., and Bloomer, S. H., 2013a, Geodynamic
830 evolution of a forearc rift in the southernmost Mariana Arc: *Island Arc*, v. 22, p. 453-
831 476.

832 Ribeiro, J. M., Ishizuka, O., Lee, C. T. A., and Girard, G., 2019, Evolution and maturation of
833 the nascent Mariana arc: *Earth and Planetary Science Letters*, v. 530, no. 115912, p.
834 <https://doi.org/10.1016/j.epsl.2019.115912>.

835 Ribeiro, J. M., Stern, R. J., Kelley, K., Shaw, A., Martinez, F., and Ohara, Y., 2015, Composition
836 of the slab-derived fluids released beneath the Mariana forearc: evidence for
837 shallow dehydration of the subducting plate: *Earth and Planetary Science Letters*, v.
838 418, p. 136–148, doi: 110.1016/j.epsl.2015.1002.1018.

839 Ribeiro, J. M., Stern, R. J., Kelley, K. A., Martinez, F., Ishizuka, O., Manton, W. I., and Ohara,
840 Y., 2013b, Nature and distribution of slab-derived fluids and mantle sources beneath
841 the Southeast Mariana forearc rift: *Geochemistry, Geophysics, Geosystems*, v. 14,
842 no. 10, p. 4585-4607.

843 Rüpke, L. H., Morgan, J. P., Hort, M., and Connolly, J. A. D., 2004, Serpentine and the
844 subduction zone water cycle: *Earth and Planetary Science Letters*, v. 223, no. 1-2, p.
845 17-34.

846 Ruscitto, D. M., Wallace, P. J., Cooper, L. B., and Plank, T., 2012, Global variations in H₂O/Ce:
847 2. Relationships to arc magma geochemistry and volatile fluxes: *Geochemistry*
848 *Geophysics Geosystems*, v. 13, no. 3, p. Q03025, DOI: 03010.01029/02011gc003887.

849 Saal, A. E., Hauri, E. H., Langmuir, C. H., and Perfit, M. R., 2002, Vapour undersaturation in
850 primitive mid-ocean-ridge basalt and the volatile content of Earth's upper mantle:
851 *Nature*, v. 419, no. 6906, p. 451-455.

852 Sadofsky, S. J., and Bebout, G. E., 2003, Record of forearc devolatilization in low-T, high-P/T
853 metasedimentary suites: Significance for models of convergent margin chemical
854 cycling: *Geochemistry, Geophysics, Geosystems*, v. 4, no. 4, p. 9003,
855 doi:9010.1029/2002GC000412.

856 Savov, I. P., Ryan, J. G., D'Antonio, M., and Fryer, P., 2007, Shallow slab fluid release across
857 and along the Mariana arc-basin system: Insights from geochemistry of serpentized
858 peridotites from the Mariana fore arc: *Journal of Geophysical Research*, v. 112, no.
859 B9, p. B09205, DOI: 09210.01029/02006JB004749.

860 Scambelluri, M., Bottazzi, P., Trommsdorff, V., Vannucci, R., Hermann, J., Gómez-Pugnaire,
861 M. T., and López-Sánchez Vizcaino, V., 2001, Incompatible element-rich fluids
862 released by antigorite breakdown in deeply subducted mantle: *Earth and Planetary
863 Science Letters*, v. 192, no. 3, p. 457-470.

864 Schiano, P., 2003, Primitive mantle magmas recorded as silicate melt inclusions in igneous
865 minerals: *Earth-Science Reviews*, v. 63, no. 1–2, p. 121-144.

866 Schmidt, M., and Poli, S., 1998, Experimentally based water budgets for dehydrating slabs
867 and consequences for magma generation: *Earth and Planetary Science Letters*, v.
868 163, no. 1-4, p. 361-379.

869 Shervais, J. W., Reagan, M., Haugen, E., Almeev, R. R., Pearce, J. A., Prytulak, J., Ryan, J. G.,
870 Whattam, S. A., Godard, M., Chapman, T., Li, H., Kurz, W., Nelson, W. R., Heaton, D.
871 E., Kirchenbaur, M., Shimizu, K., Sakuyama, T., Li, Y., and Vetter, S. K., 2019,
872 Magmatic Response to Subduction Initiation: Part 1. Fore-arc Basalts of the Izu-Bonin
873 Arc From IODP Expedition 352: *Geochemistry Geophysics Geosystems*, v. 20, no. 1, p.
874 314-338.

875 Shervais, J. W., Reagan, M. K., Godard, M., Prytulak, J., Ryan, J. G., Pearce, J. A., Almeev, R.
876 R., Li, H., Haugen, E., Chapman, T., Kurz, W., Nelson, W. R., Heaton, D. E.,
877 Kirchenbaur, M., Shimizu, K., Sakuyama, T., Vetter, S. K., Li, Y., and Whattam, S. A.,
878 2021, Magmatic Response to Subduction Initiation, Part II: Boninites and Related
879 Rocks of the Izu-Bonin Arc From IOPD Expedition 352: *Geochemistry Geophysics
880 Geosystems*, v. 22, no. 1, p. e2020GC009093,
881 <https://doi.org/009010.001029/002020GC009093>.

882 Stern, R. J., and Bloomer, S. H., 1992, Subduction zone infancy: Examples from the Eocene
883 Izu-Bonin-Mariana and Jurassic California arcs: *Geological Society of America
884 Bulletin*, v. 104, no. 12, p. 1621-1636.

885 Stern, R. J., Fouch, M., and Klemperer, S. L., 2003, An Overview of the Izu-Bonin-Mariana
886 Subduction Factory, *in* Eiler, J., and Hirschmann, M., eds., *Inside the subduction
887 factory*, Volume 138: Washington, D.C., *Geophysical Monograph Series*, p. 175-222.

888 Stern, R. J., Tamura, Y., Ishizuka, O., Shukano, H., Bloomer, S. H., Embley, R. W., Leybourne,
889 M., Kawabata, H., Nunokawa, A., Nichols, A. R. L., Kohut, E., and Pujana, I., 2013a,
890 Volcanoes of the Diamante cross-chain: evidence for a mid-crustal felsic magma
891 body beneath the Southern Izu–Bonin–Mariana arc: *Geological Society, London,
892 Special Publications*, v. 385, <https://doi.org/10.1144/SP385.6>.

893 Stern, R. J., Tamura, Y., Masuda, H., Fryer, P., Martinez, F., Ishizuka, O., and Bloomer, S. H.,
894 2013b, How the Mariana Volcanic Arc ends in the south: *Island Arc*, v. 22, p. 133-148.

895 Straub, S. M., Goldstein, S. L., Class, C., Schmidt, A., and Gomez-Tuena, A., 2010, Slab and
896 Mantle Controls on the Sr–Nd–Pb–Hf Isotope Evolution of the Post 42 Ma Izu–Bonin
897 Volcanic Arc: *Journal of Petrology*, v. 51, no. 5, p. 993-1026.

898 Straub, S. M., Woodhead, J. D., and Arculus, R. J., 2015, Temporal Evolution of the Mariana
899 Arc: Mantle Wedge and Subducted Slab Controls Revealed with a Tephra
900 Perspective: *Journal of Petrology*, v. 56, no. 2, p. 409-439.

901 Tamura, Y., Ishizuka, O., Stern, R. J., Nichols, A. R. L., Kawabata, H., Hirahara, Y., Chang, Q.,
902 Miyazaki, T., Kimura, J., Embley, R. W., and Tatsumi, Y., 2014, Mission Immiscible:
903 Distinct Subduction Components Generate Two Primary Magmas at Pagan Volcano,
904 Mariana Arc: *Journal of Petrology*, v. 55, no. 1, p. 63-101.

905 Tamura, Y., Ishizuka, O., Stern, R. J., Shukuno, H., Kawabata, H., Embley, R. W., Hirahara, Y.,
906 Chang, Q., Kimura, J.-I., Tatsumi, Y., Nunokawa, A., and Bloomer, S. H., 2011, Two

907 Primary Basalt Magma Types from Northwest Rota-1 Volcano, Mariana Arc and its
908 Mantle Diapir or Mantle Wedge Plume: Journal of Petrology, v. 52, no. 6, p. 1143-
909 1183.
910

911 **Figure captions**

912 **Fig. 1: Subduction inception vs. modern near-trench spreading.** A) Sketch of near-
913 trench spreading that occurred during subduction inception, such as in the Eocene IBM proto-
914 arc crust. B) Sketch of the Southern Mariana fore-arc rifts (SEMFR), which represents a
915 modern near-trench spreading center that developed in the fore-arc above a mature
916 subduction zone in Pliocene time. The Southern Mariana is characterized by the occurrence
917 of infant arc volcanoes (the Fina-Nagu volcanic chain) and a back-arc basin (BAB) spreading
918 center, the Malaguana-Gadao Ridge (MGR). Although the SEMFR share some similarities
919 with the IBM proto-arc crusts, these geological features are not observed during subduction
920 inception; and they are instead typical of long-lived subduction zones.
921

922 **Fig. 2: Bathymetric map of the Izu-Bonin-Mariana convergent margin**
923 (<http://www.geomapapp.org>). The map shows the location of the IODP Site 352 (Reagan et
924 al., 2017), Bonin Island (Ishizuka et al., 2020; Kanayama et al., 2012, 2014), southern
925 Mariana fore-arc rifts (SEMFR) (Ribeiro et al., 2013a; Ribeiro et al., 2013b), and of the
926 Eocene proto-arc crust from the southern Marianas (Reagan et al., 2010).
927

928 **Fig. 3: Composition of the magmas.** A) SiO₂ vs. K₂O diagram used to classify rocks
929 (Peccerillo and Taylor, 1976). B) MgO vs. TiO₂ diagram. The southern Mariana olivine-
930 hosted melt inclusions are primitive basalts with a boninitic fingerprint. The boninitic
931 compositional field is from Pearce and Reagan (2019). C-D) MgO vs. SiO₂ classification
932 diagram of Pearce and Reagan (2019) used to distinguish low- and high-Si boninites. We
933 compiled glass shards and olivine-hosted melt inclusions for the IBM proto-arc magmas and
934 for the SEMFR magmas to ensure freshness, and bulk rocks for the IBM infant arc as there
935 were no available data for basaltic glass shards. White numbers in black circles (from 1 to 5)
936 refers to the compositional evolution of the magma over time. These numbers also refer to
937 the sequence of event the caption, as well as to the sequence of events outlined in the
938 discussion.
939

940 **Fig. 4: Composition of the slab fluids released during subduction inception.** A) Th/Nb vs.
941 Nb/Yb and B) Ba/Th vs. Rb/Th diagrams, after Pearce et al. (2005), showing enrichments in
942 sediment melts (Th/Nb) and in water-rich, slab fluids (Ba/Th, Rb/Th) in the magmas. The
943 IBM boninites and the SEMFR basalts and associated olivine-hosted melt inclusions display
944 high slab fluid markers in Rb/Th and Ba/Th, indicating that they captured water-rich slab
945 fluids. The light green, dark green and blue rectangles represent the fluid composition (water-
946 rich fluid and solute-rich fluid) released from the subducted sediments (sed.), the subducted
947 serpentinites, and the altered oceanic crust (AOC), respectively. The composition of the slab
948 fluids were assessed using the bulk sediment composition of the Mariana composite, Site 800
949 (Plank and Langmuir, 1998) and the partition coefficients for melting and dehydration of the
950 subducted sediments (Johnson and Plank, 1999), the composition of the crust composite of
951 Site 801 (“SUPER”) (Kelley et al., 2003) and the partition coefficients for dehydrating the
952 oceanic crust (Kessel et al., 2005), and the composition of olivine-hosted fluid inclusions
953 from serpentinitized mantle rocks (Ribeiro et al., 2015). See text and Table S2 for details.
954

955 **Fig. 5: Composition of the water-rich slab fluids released during subduction inception.**
956 A) H₂O/Ce, B) Cs/Th and C) Cs/Ba vs Rb/Th diagrams showing the strong enrichment in
957 water-rich slab fluids of the SEMFR basalts and proto-arc boninites glasses from IBM, as
958 compared to the IBM arc and back-arc basalts. The light green, dark green and blue
959 rectangles represent the slab fluid composition released from the subducted sediments (sed.),
960 the subducted serpentinites, and the altered oceanic crust (AOC), respectively. See Fig. 3 for
961 details about the slab fluid composition.

962
963 **Fig. 6: Melting of the oceanic crust in the amphibolite facies during subduction**
964 **inception.** A) Zr/Sm and B) Hf/Sm vs. La/Sm diagrams of Pearce et al. (1992) showing that
965 melts from the oceanic crust infiltrated the depleted mantle source of the low-silica and high-
966 silica boninites in IBM.

967
968 **Fig. 7: Variations of the water-rich slab fluids with the distance to the trench in IBM.** A)
969 H₂O/Ce and B) Rb/Th vs. trench distance. The highest H₂O/Ce and Rb/Th ratios in the IBM
970 boninites suggest that there is a peak in slab dehydration in IBM within 1-2 Myr after the
971 onset of subduction, which rapidly decreases with time and trench distance, as the arc
972 develops. Similar ratios are also observed in the SEMFR magmas, indicating that a peak in
973 slab dehydration may also occur within 90 km from the trench in long-lived, cold subduction
974 zones (Johnson and Plank, 1999). We used the estimated distance to the trench for the IBM
975 FABs (~20- 30 km) and IBM boninites (~40 - 60 km) of Reagan et al. (2019). The trench
976 distance for the infant arc (~80 ± 25 km) was assessed from the current location of Hahajima
977 (Ishizuka et al., 2020), which represent preserved infant arc volcanoes that formed in Eocene
978 time. A trench distance of 200 ± 25 km was estimated for the Mariana arc, and of 300 ± 25
979 km for the Mariana Trough. Trench distance for the SEMFR glasses (± 5 km) is from Ribeiro
980 et al. (2013a).

981
982 **Fig. 8: Sources of the slab fluids throughout the lifetime of IBM.** A) Ba/Th vs. ²⁰⁶Pb/²⁰⁴Pb
983 and B) Ba/Th vs. ⁸⁷Sr/⁸⁶Sr diagrams show that the subducted mantle and the altered oceanic
984 crust dehydrate first to contribute to fingerprint the IBM boninites. The composition of the
985 subducted sediments in ²⁰⁶Pb/²⁰⁴Pb cannot explain the compositional variations observed in
986 the magmas (panel A). C) Th/Nb vs. ²⁰⁶Pb/²⁰⁴Pb and D) vs. ²⁰⁷Pb/²⁰⁶Pb diagrams showing
987 the enrichment in sediment melts into the mature arc magmas. D) We used bulk rock
988 composition for all samples as radiogenic isotopes were not measured on glass shards.
989 Because Ba, Th and Nb are less sensitive to secondary alteration processes than Cs and Rb,
990 Ba/Th, and Th/Nb were used to track the slab fluid contribution. Details about the end-
991 members and the mixing equations are provided in the supplementary material and in Table
992 S2. AOC: altered oceanic crust, sed: sediments, serp: serpentinitized mantle. The black start
993 represents the estimated mantle composition of Ribeiro et al. (2013b).

994
995 **Fig. 9: Sources of the slab fluids in the SEMFR magmas.** A) Ba/Th vs. ²⁰⁶Pb/²⁰⁴Pb and B)
996 vs. ⁸⁷Sr/⁸⁶Sr diagrams showing the contribution of the altered oceanic crust (AOC) and
997 serpentinitized mantle (serp) in the water-rich fluids released beneath the southern Mariana
998 fore-arc. C) Th/Nb vs. ²⁰⁶Pb/²⁰⁴Pb and D) vs. ²⁰⁷Pb/²⁰⁶Pb diagrams showing the reduced
999 enrichment in sediment melts into the SEMFR magmas. The composition of the SEMFR
1000 magmas overlap that of the LSB. We plotted the bulk composition of the magmas as isotopic
1001 composition were only measured in whole rocks. For this reason, we selected Ba and Th to
1002 track the slab fluids as in Pearce et al. (2005), as these elements are less prone to alteration
1003 than Cs and Rb.

1004

1005 **Fig. 10: Pb isotopic composition of the IBM and SEMFR magmas.** A-B) $^{206}\text{Pb}/^{204}\text{Pb}$ vs.
1006 $^{208}\text{Pb}/^{206}\text{Pb}$ and C-D) $^{206}\text{Pb}/^{204}\text{Pb}$ vs. $^{207}\text{Pb}/^{206}\text{Pb}$ diagrams showing the various contribution in
1007 sediments and altered oceanic crust in the SEMFR (B, D) and IBM magmas over time (A, C).
1008 The white numbers in a black circle represent the time sequence of the IBM magmas (see
1009 figure caption for details).
1010

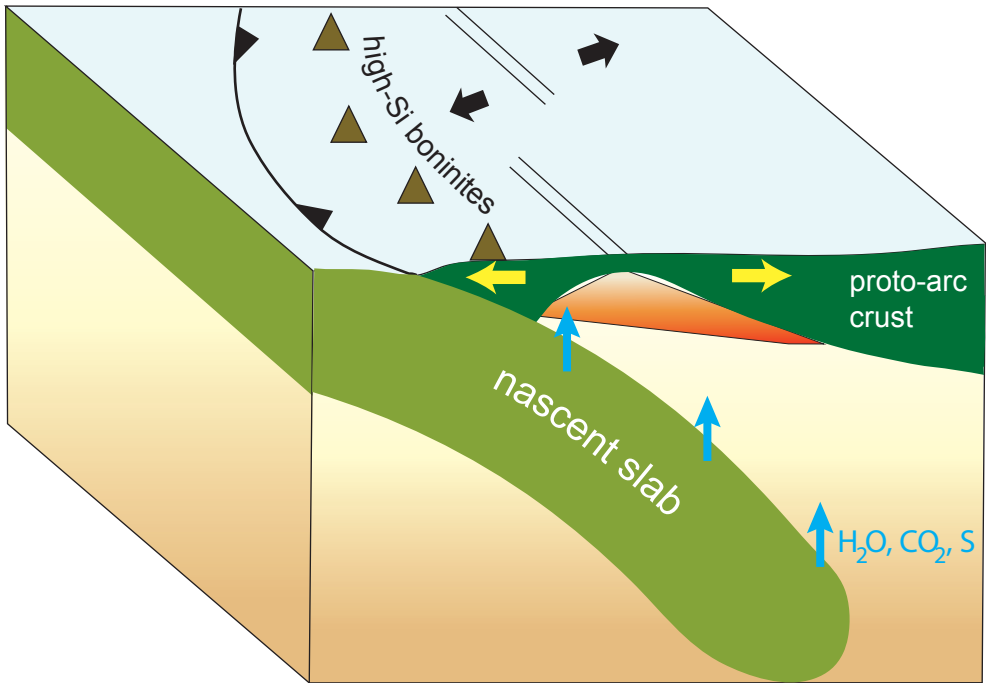
1011 **Fig. 11: Sketch illustrating slab dehydration and melting following subduction**
1012 **inception.** A) During subduction inception, FABs form by decompression melting within a
1013 few kilometers from the trench. Large fluxes of water-rich fluids are rapidly released within
1014 90 km from the trench from dehydrating the subducted mantle and the altered oceanic crust
1015 (AOC) within 2 – 3 Myr following subduction inception. The nascent, warm slab also melts
1016 in the amphibolite facies. B) In IBM, the increasing fluxing of the highly depleted mantle
1017 source produces the HSB. The HSB marks the transition from adiabatic decompression to
1018 fluid-assisted mantle melting. Eruption of the HSB terminates shortly after the development
1019 of the infant volcanic arc within 5 to 10 Ma following subduction inception. The slab
1020 capacity to carry volatiles diminishes with increasing slab depth, so that the infant arc
1021 magmas capture less water-rich slab fluids, as they are migrating away from the trench. C) As
1022 the volcanic arc front reach maturation, the IBM volcanic arc front is at ~200 km from the
1023 trench and capture slab fluids released from a deeper part of the slab. The deeper slab fluids
1024 are less enriched in water (Rb, Cs) and more enriched in total dissolved solutes and K. The
1025 contribution of the sediment melts into the arc magmas thus increases with time and
1026 increasing slab depth. This evolution and subsequent stabilization of the subduction zone is
1027 permitted by slab dehydration at shallow depth, that is associated serpentinization of the fore-
1028 arc mantle since arc inception.
1029

1030 **Supplementary material**

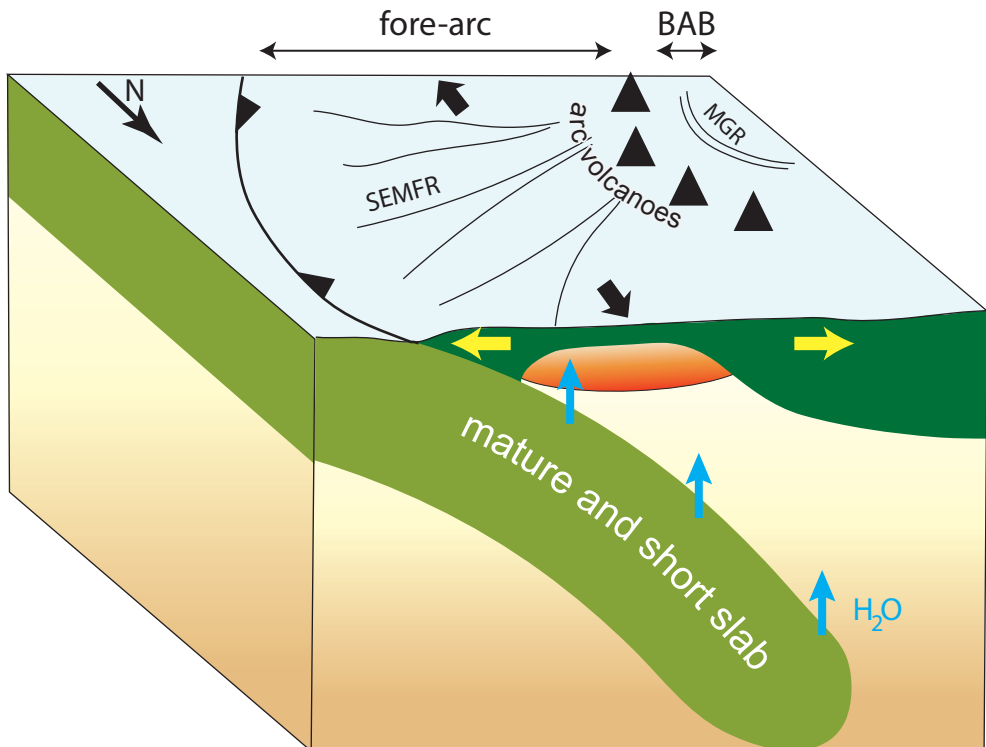
1031
1032 **Table S1:** Compiled dataset for major and trace element composition of the fresh glass
1033 shards and olivine-hosted melt inclusions from the Southern Marianas, the Mariana arc and
1034 back-arc basin, and the Izu-Bonin-Mariana proto-arc crust.
1035

1036 **Table S2:** Composition of the end-members and slab fluid composition used for the mixing
1037 equations.
1038

A- Subduction inception



B- SEMFR: modern near-trench spreading



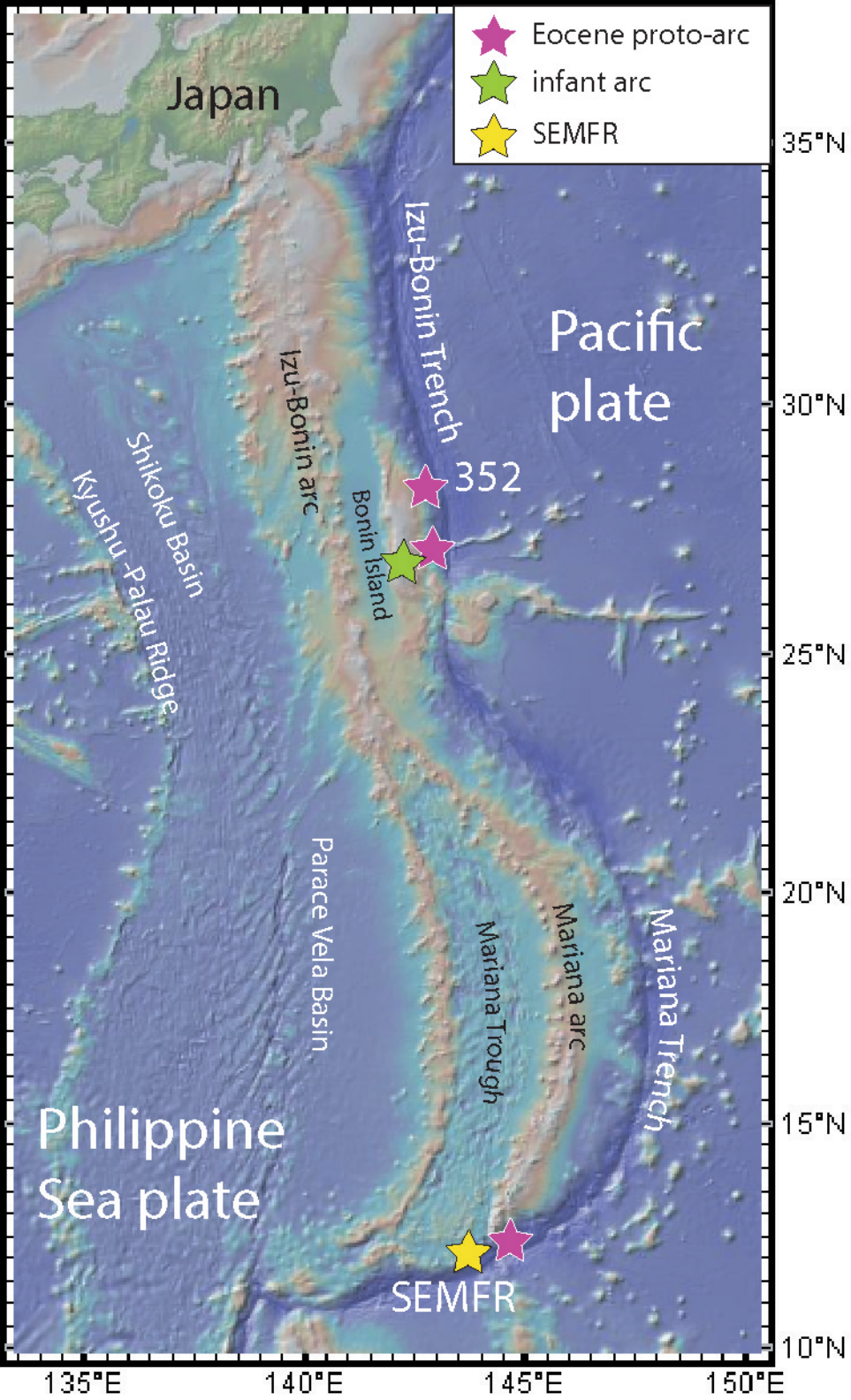
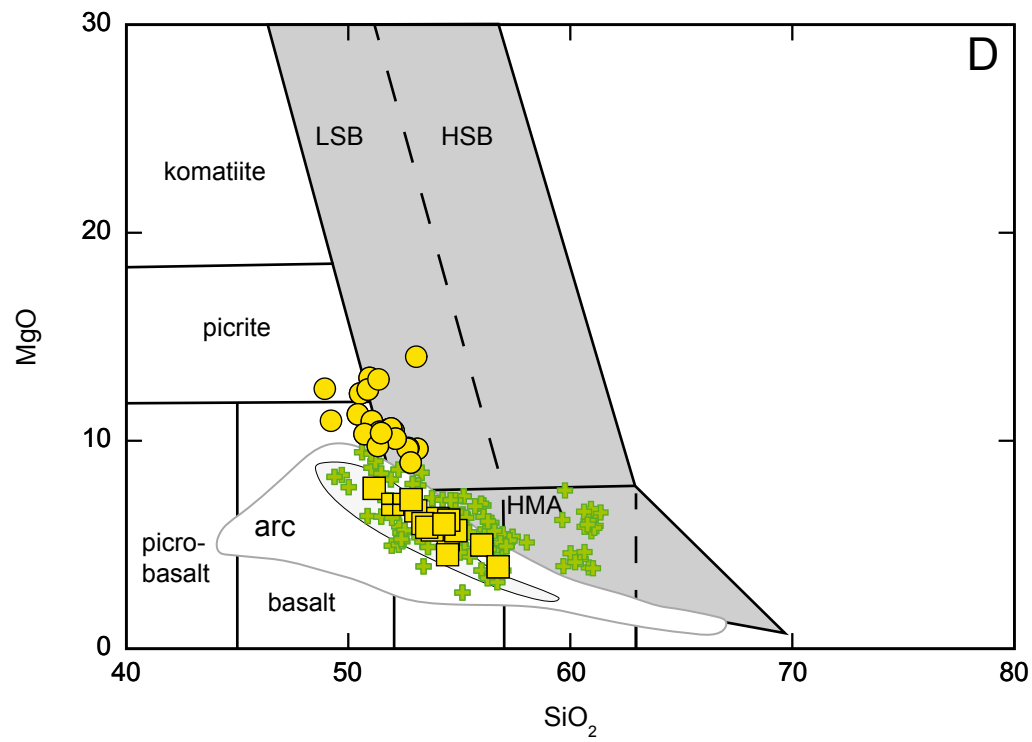
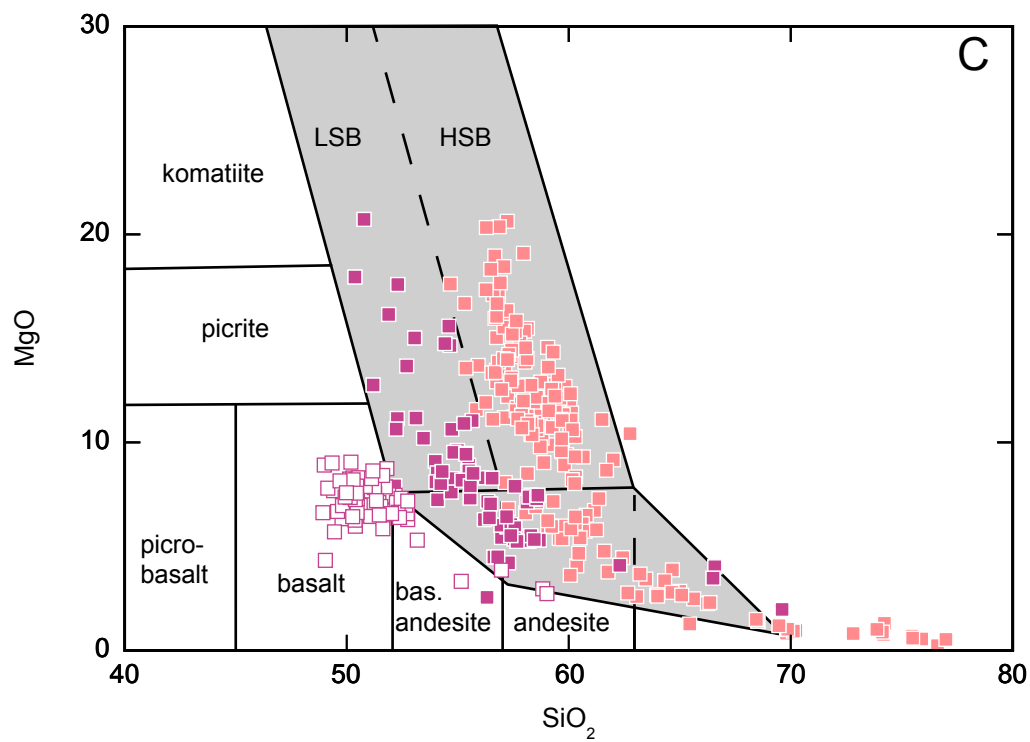
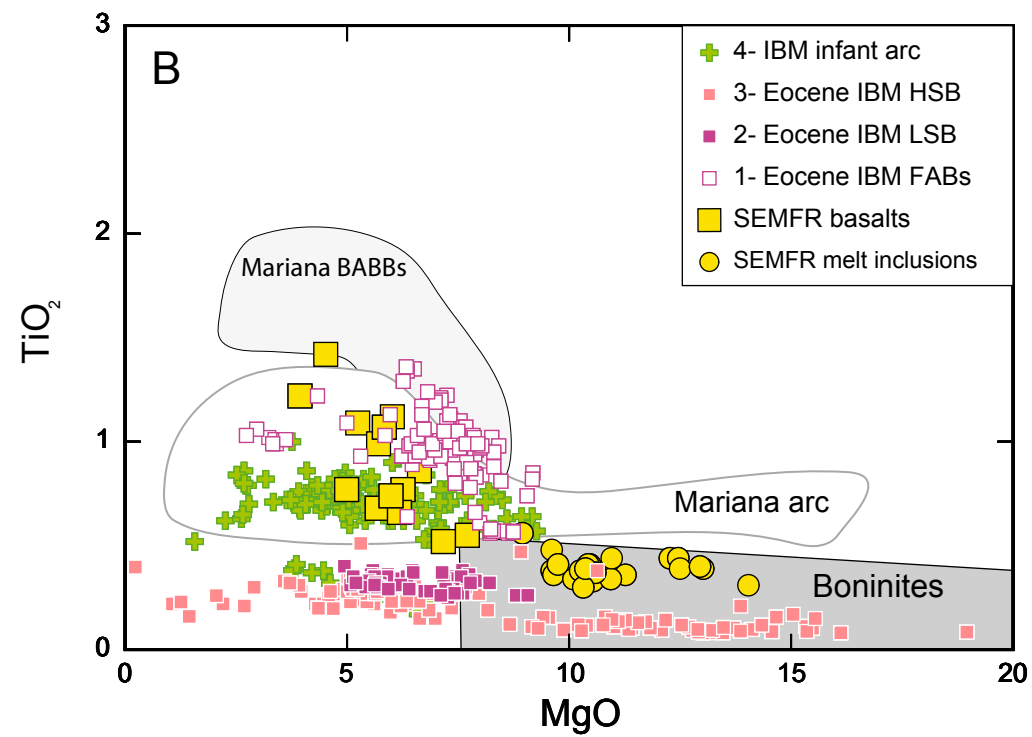
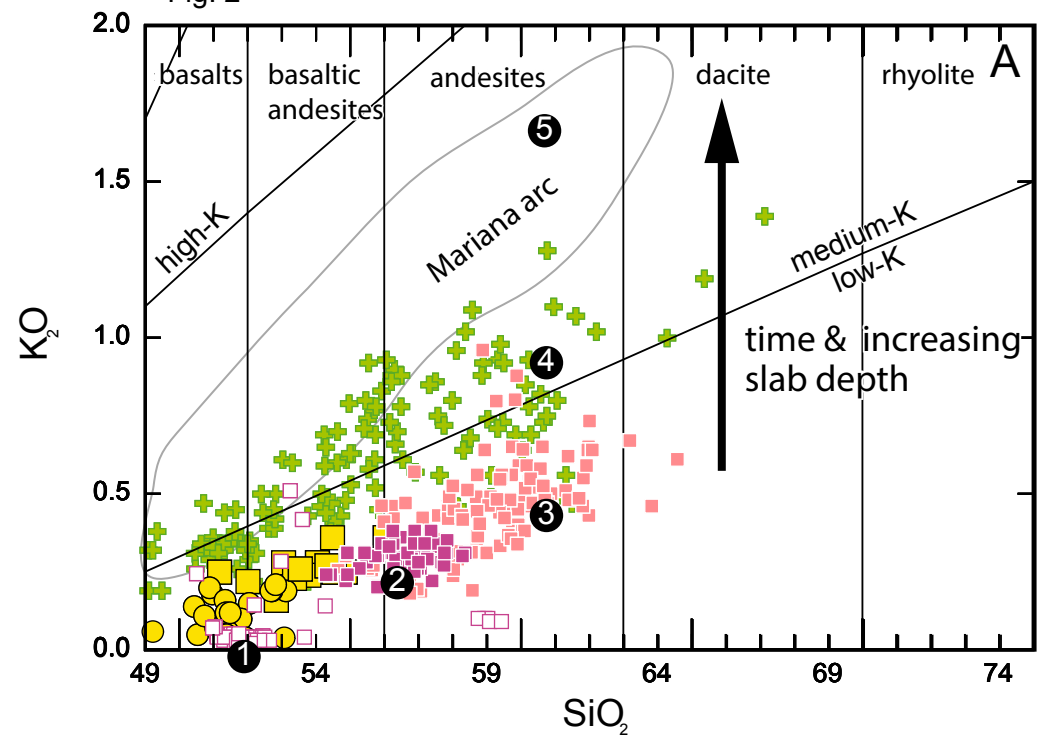
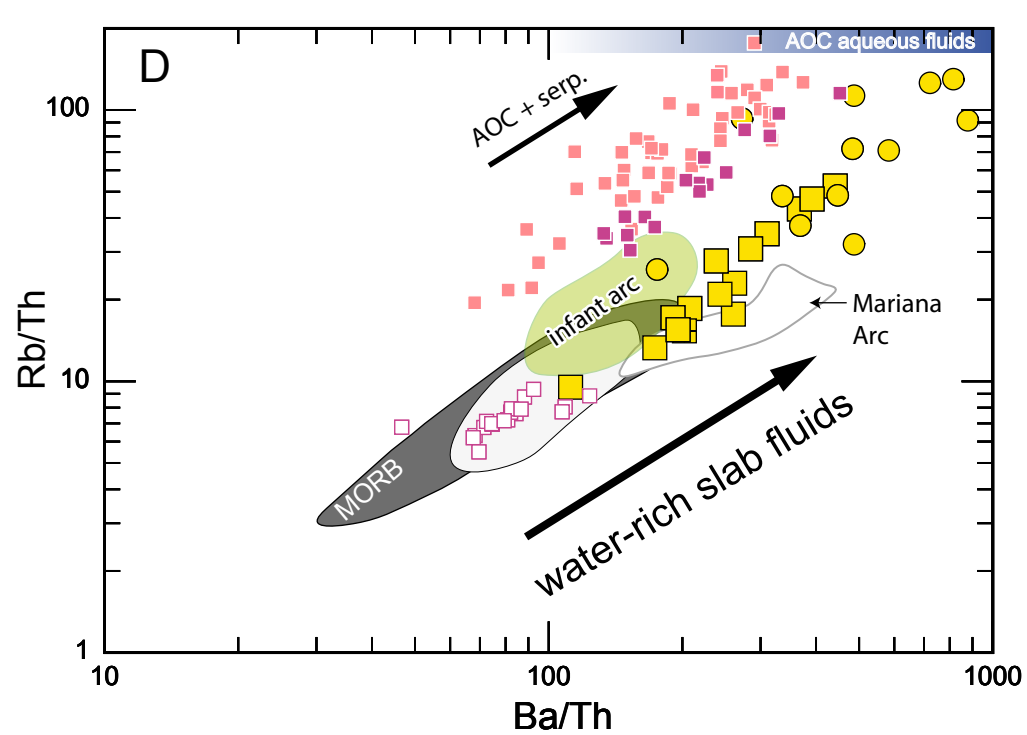
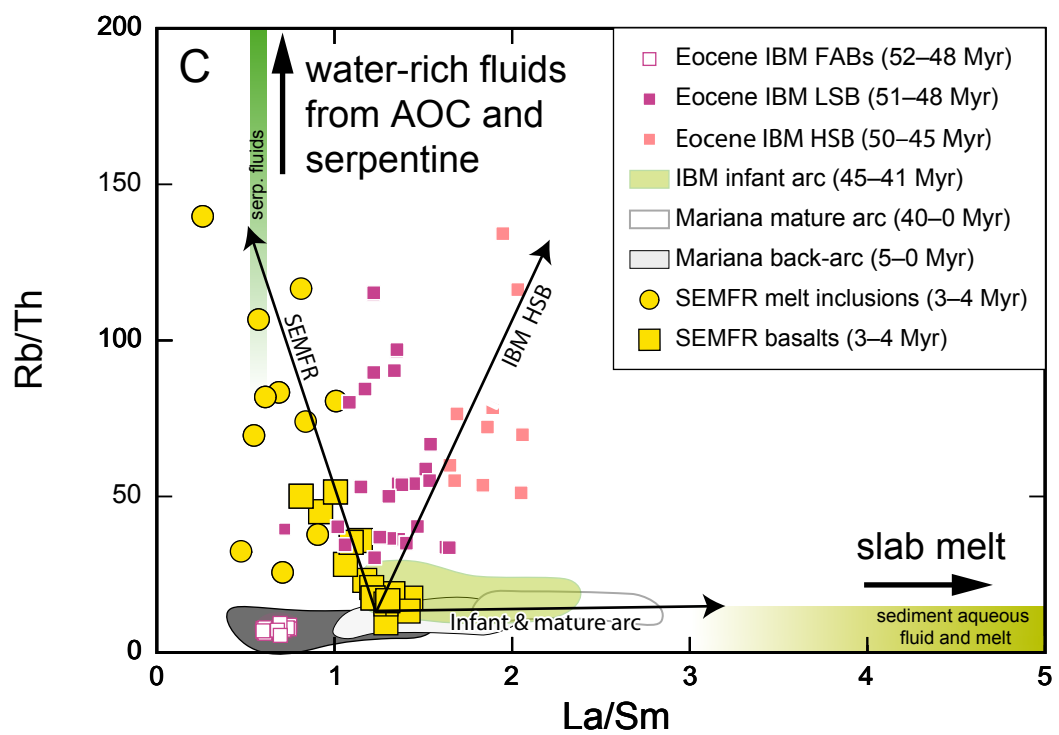
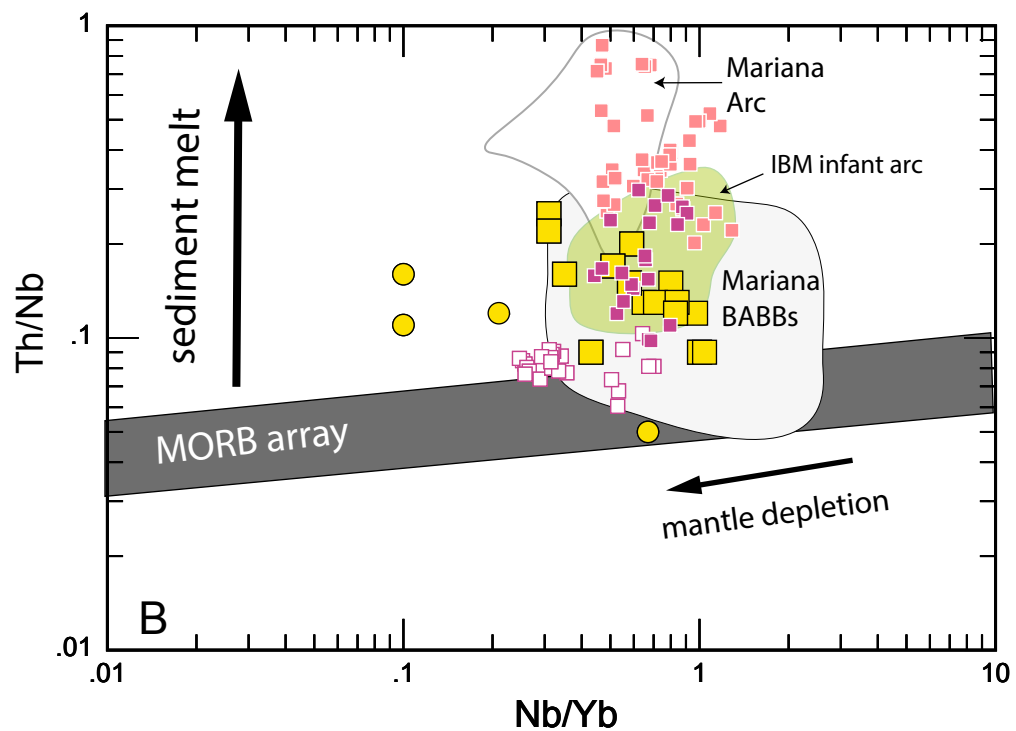
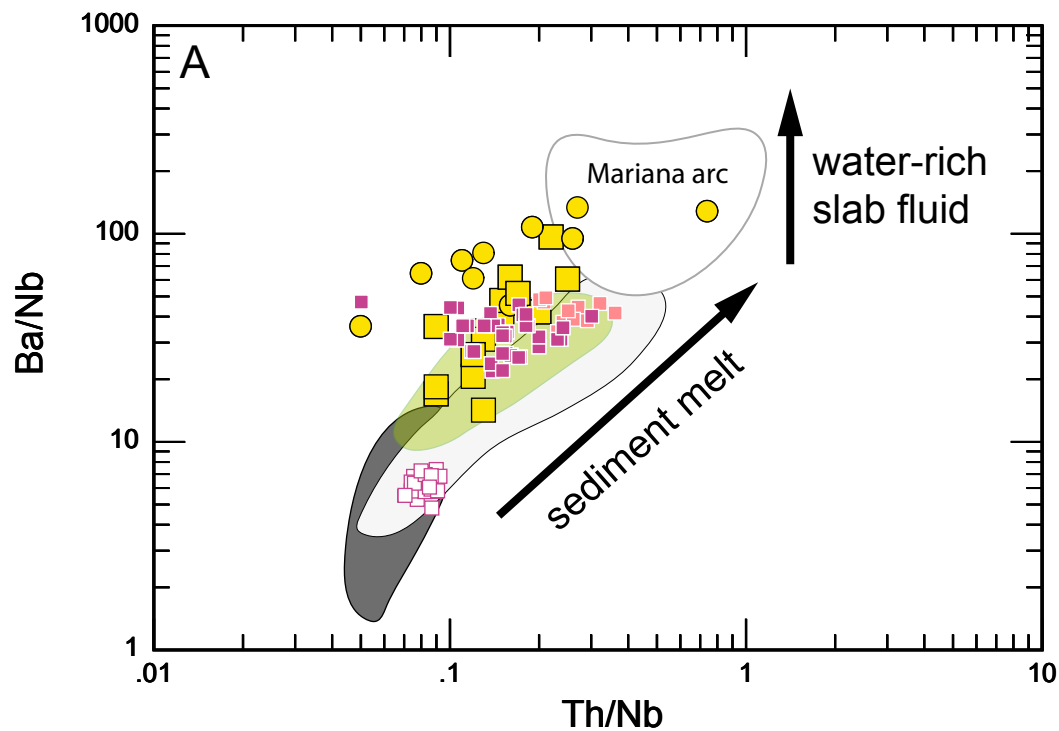


Fig. 2





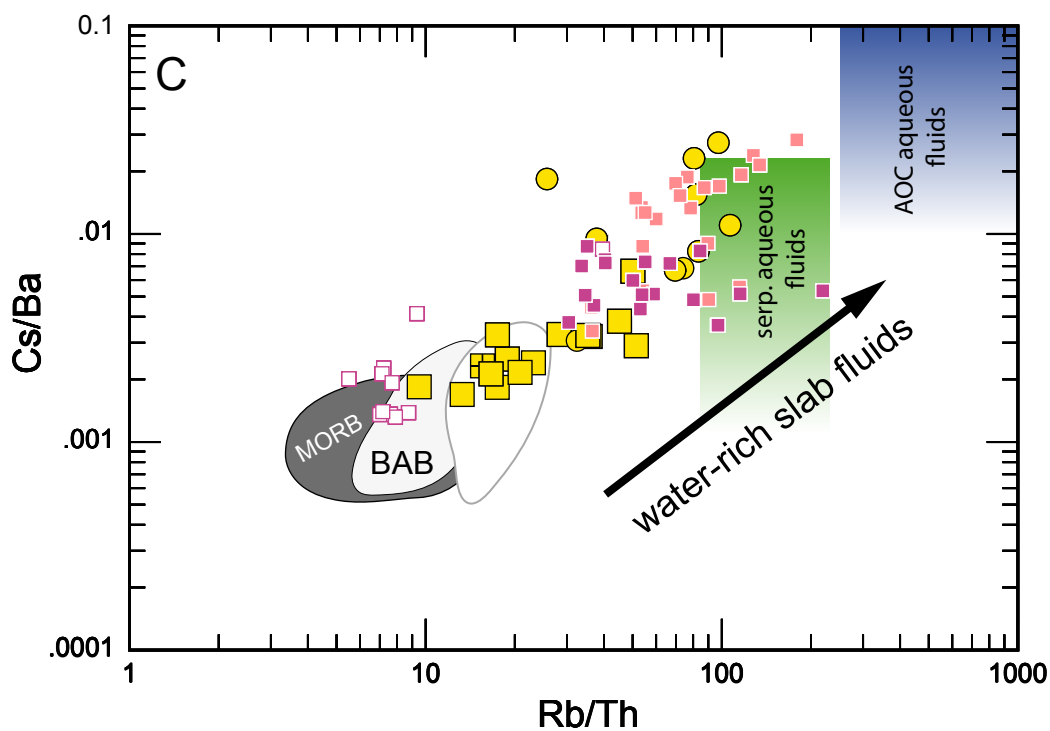
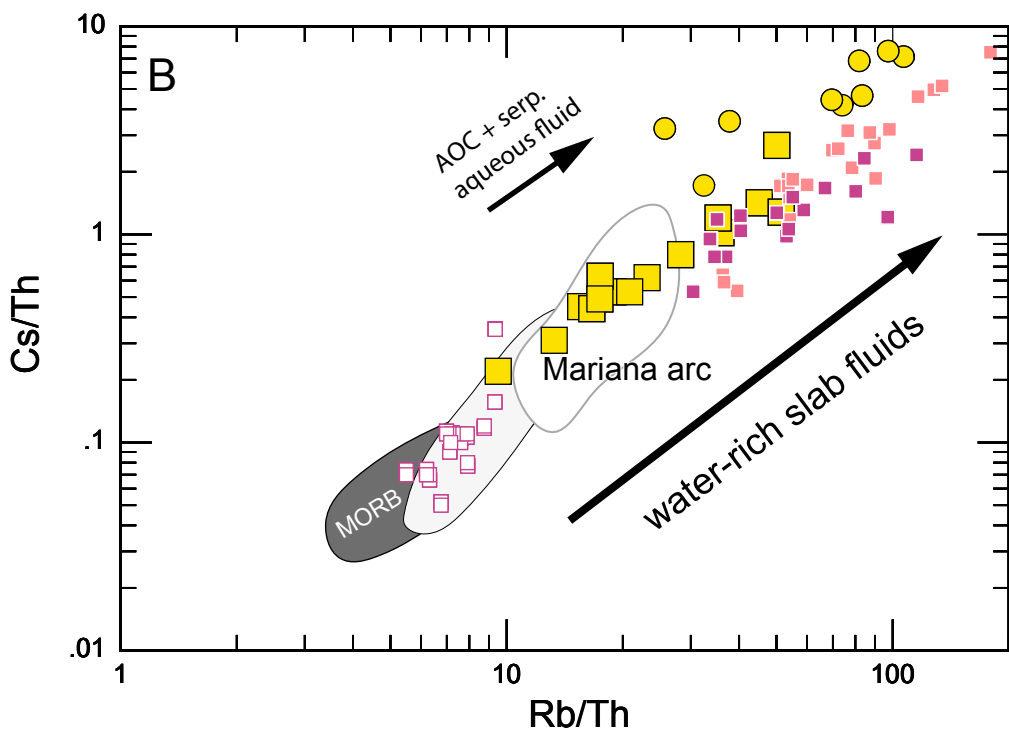
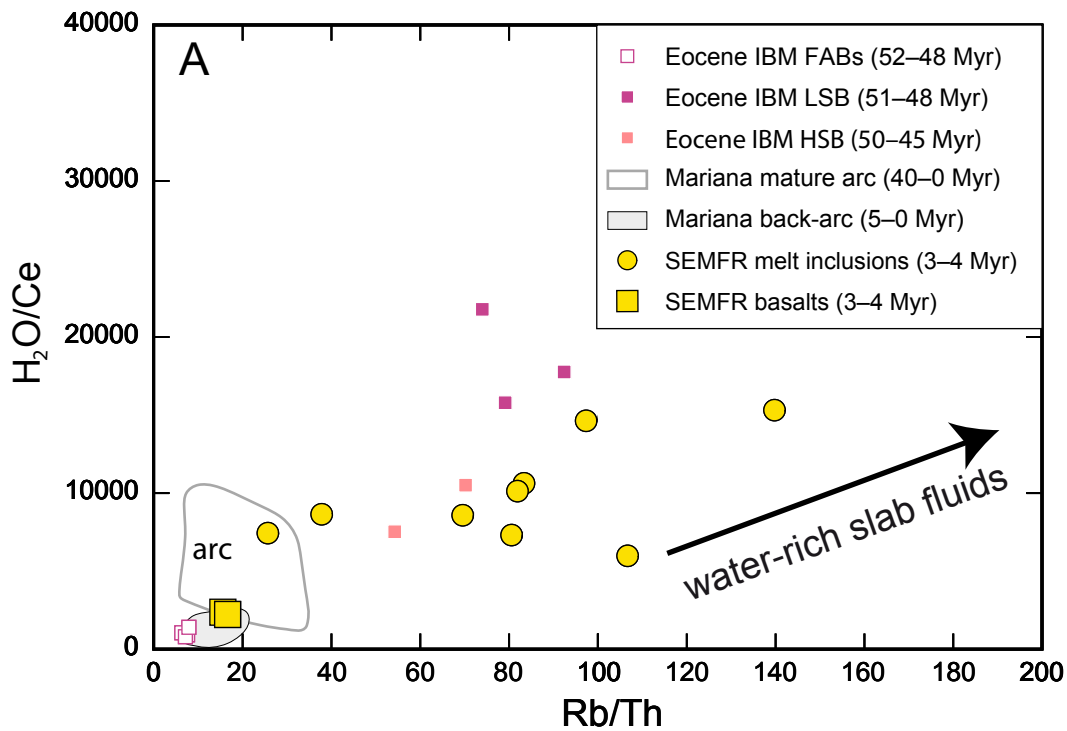
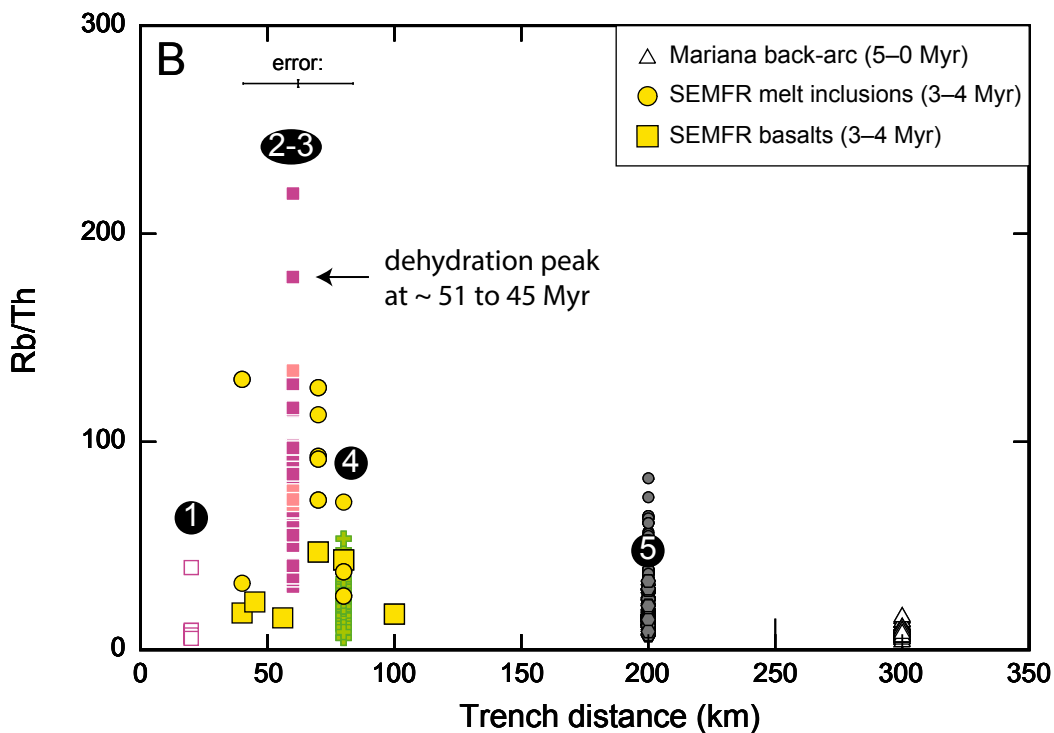
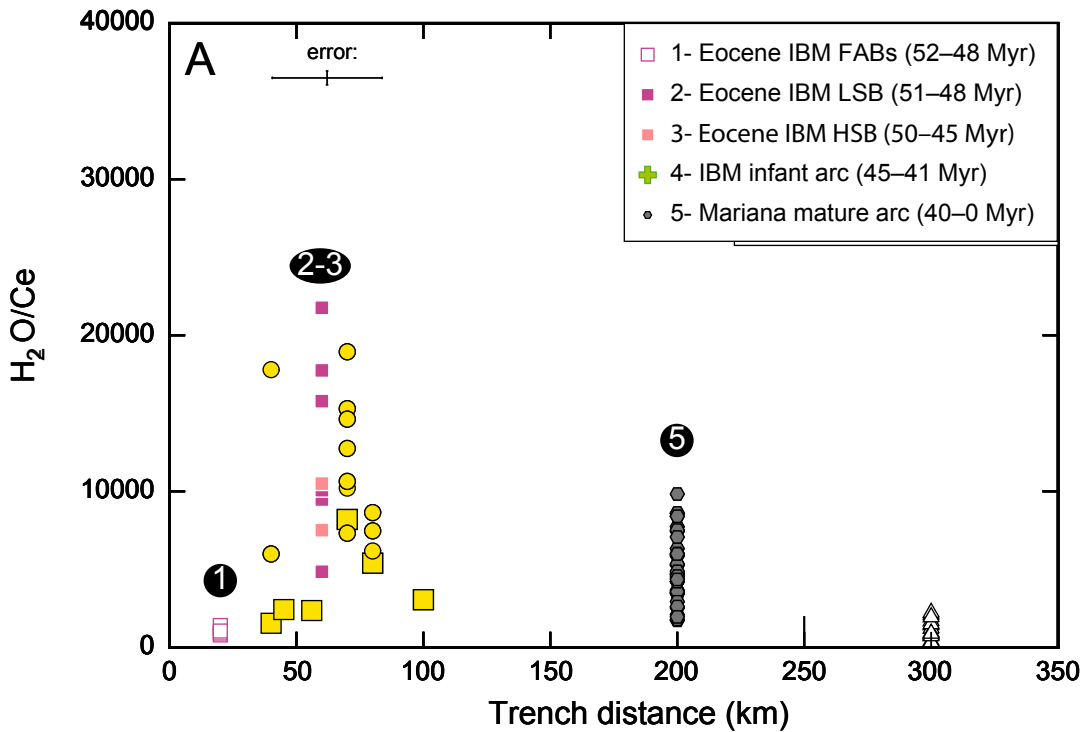
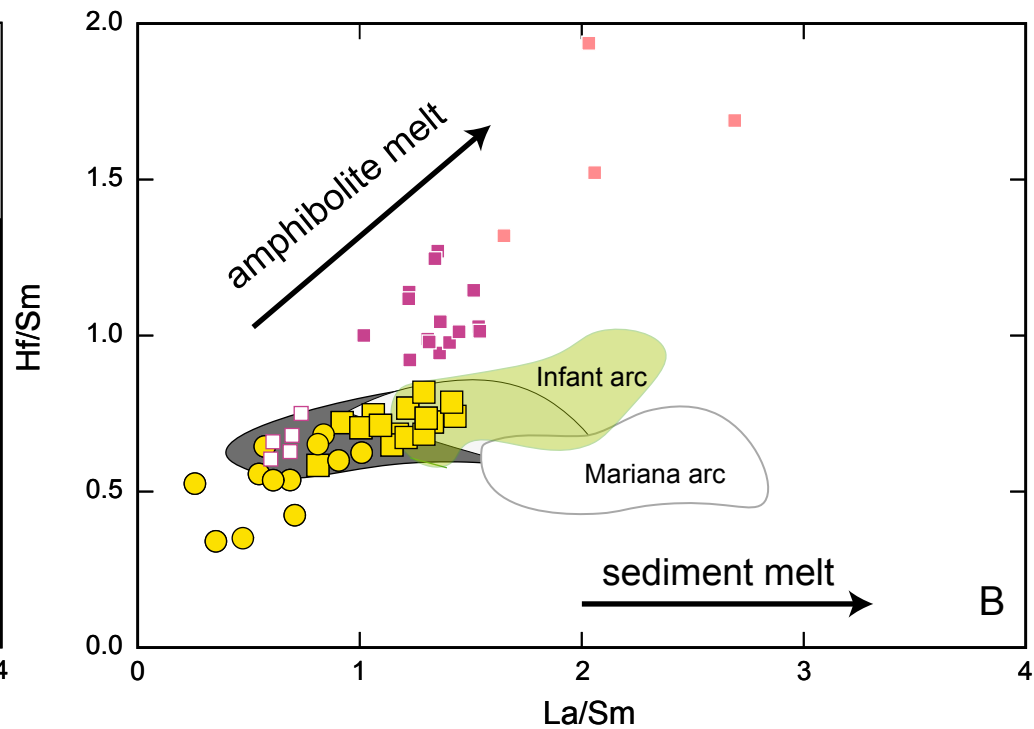
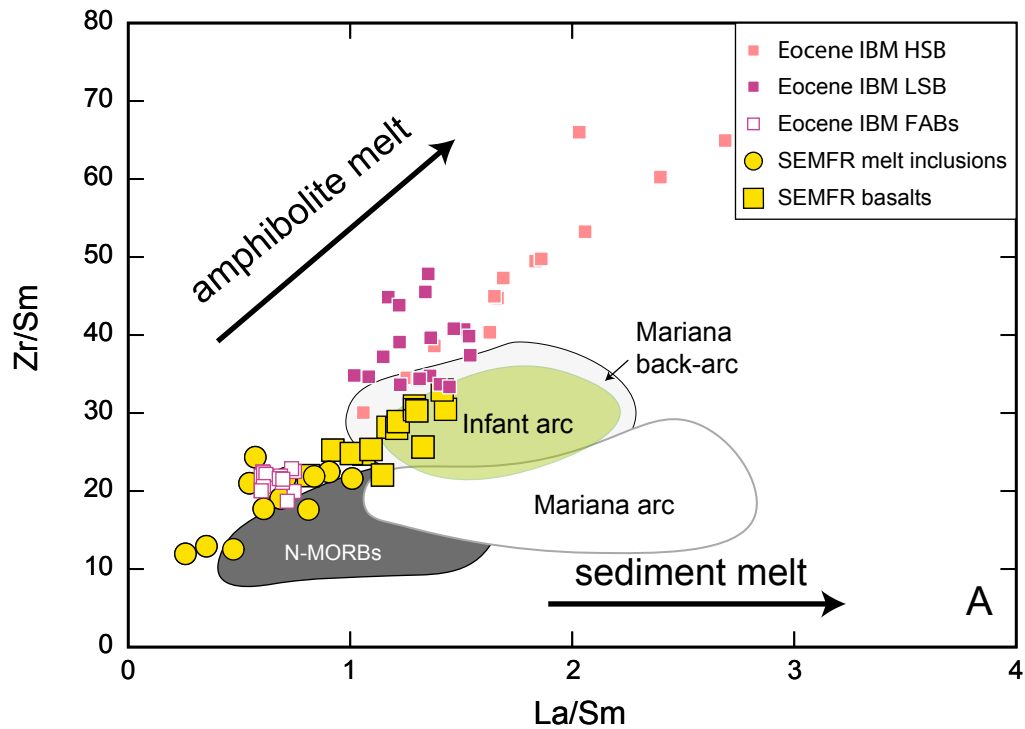


Fig. 6





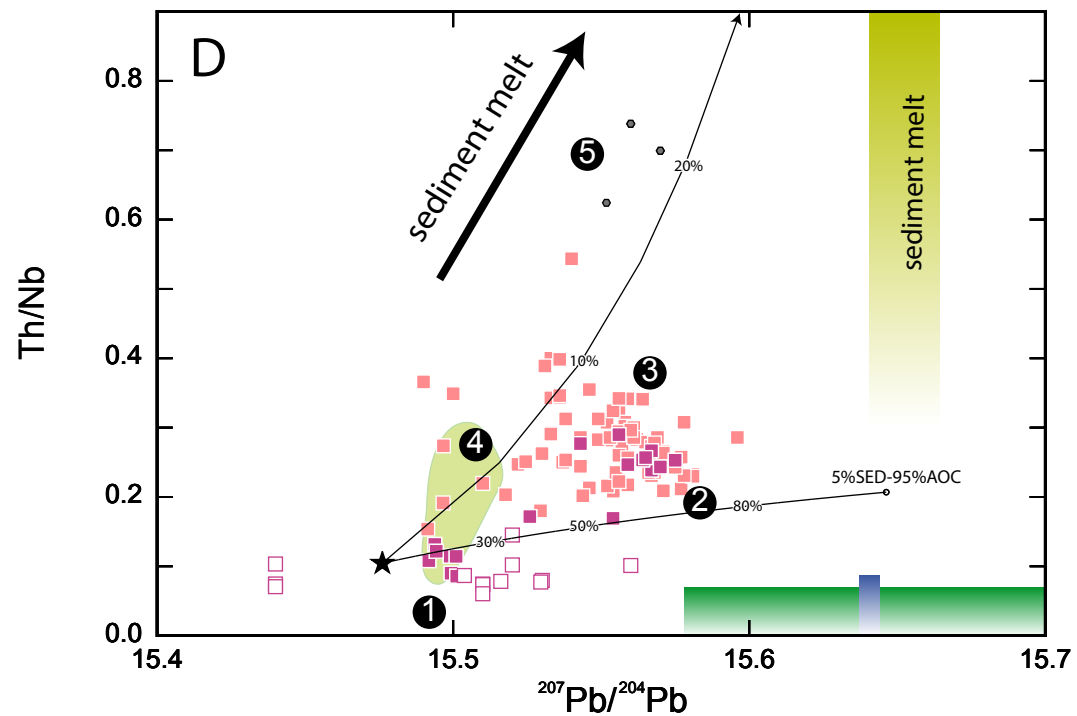
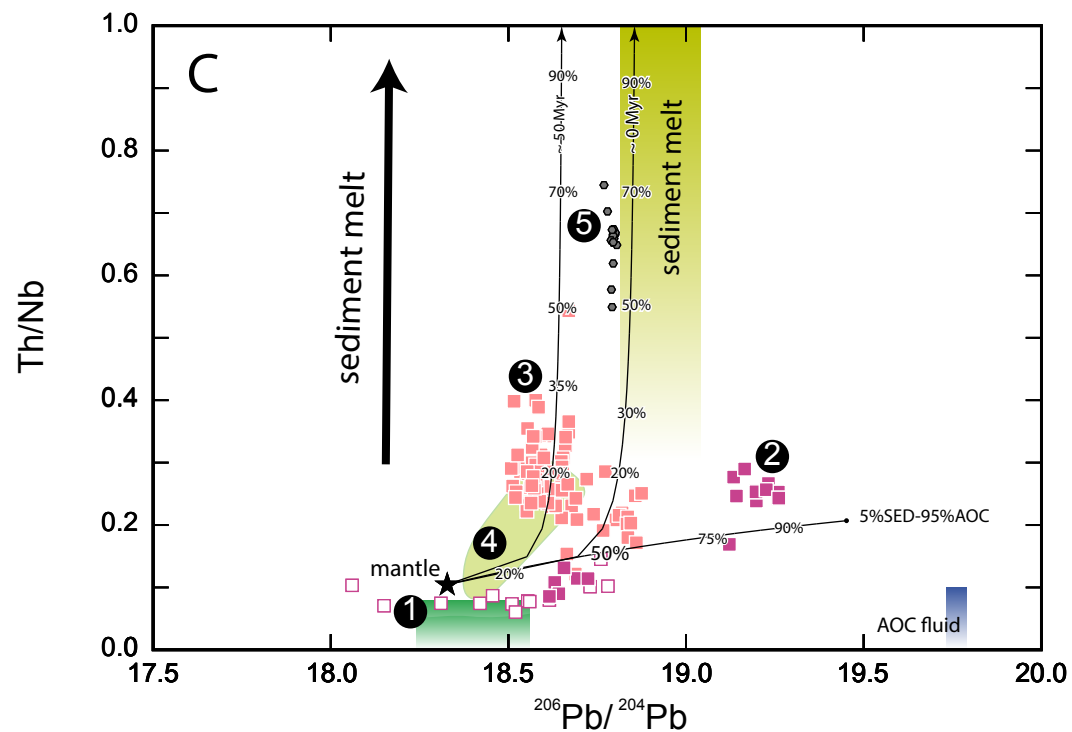
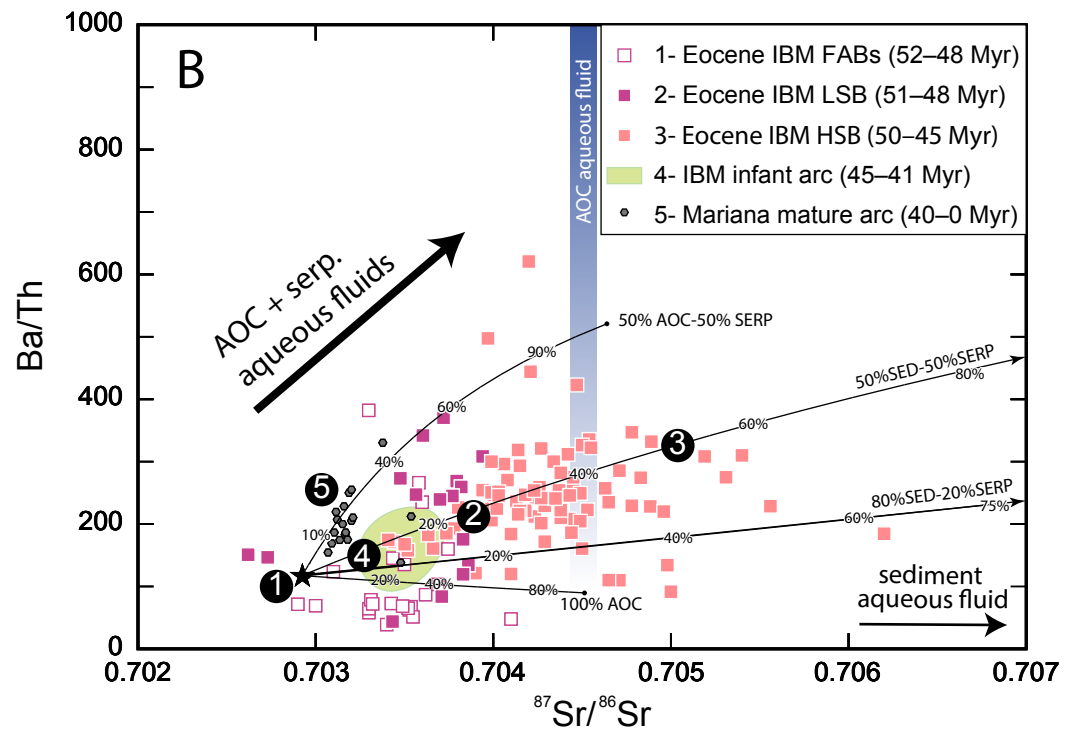
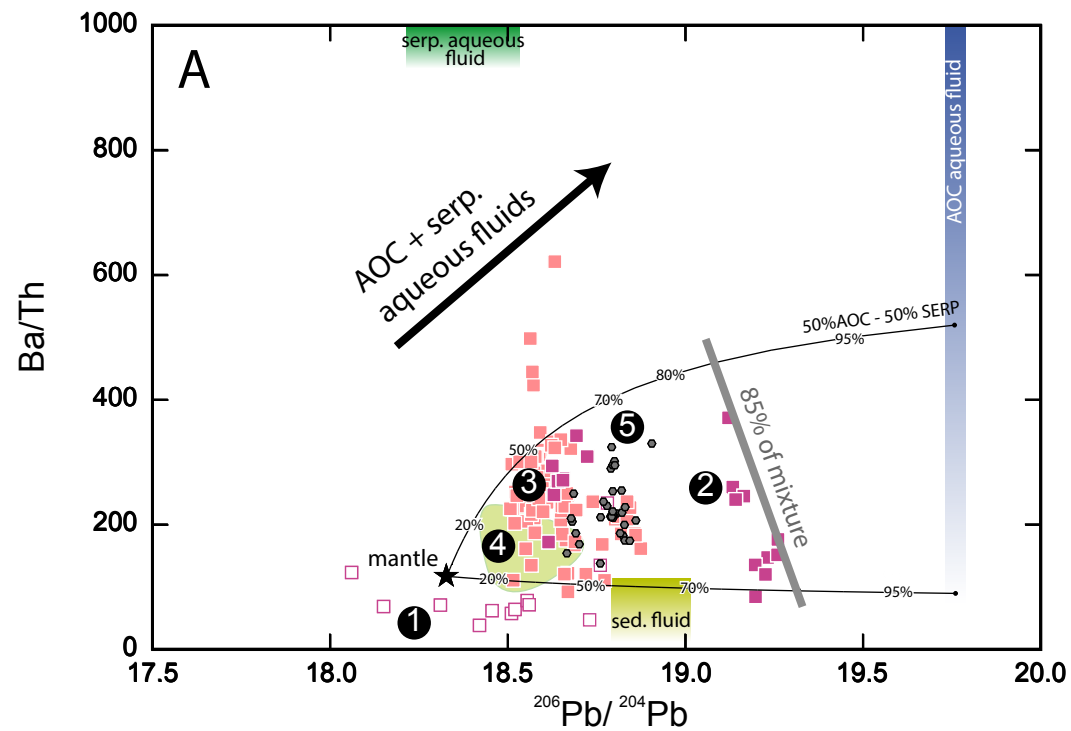
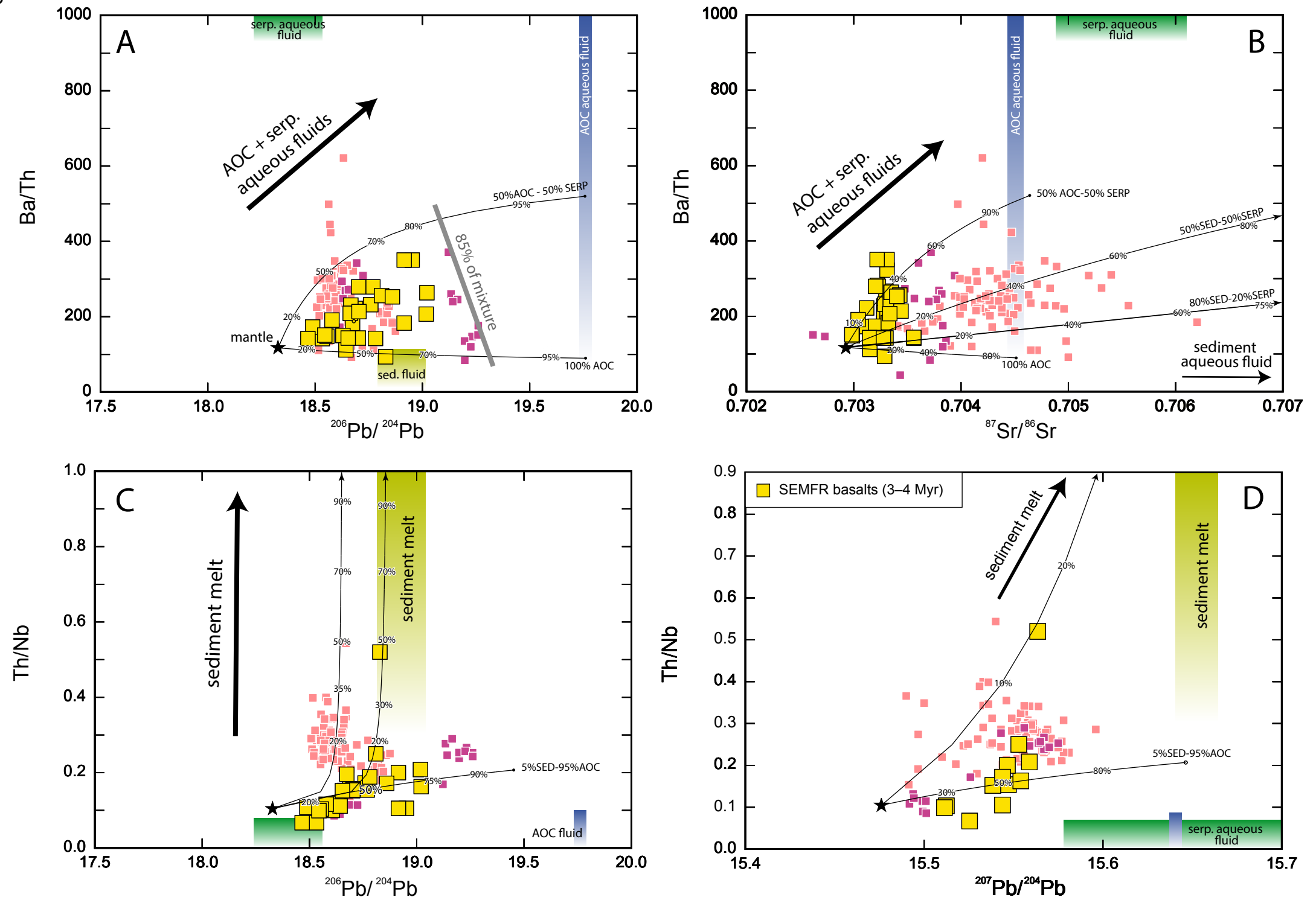
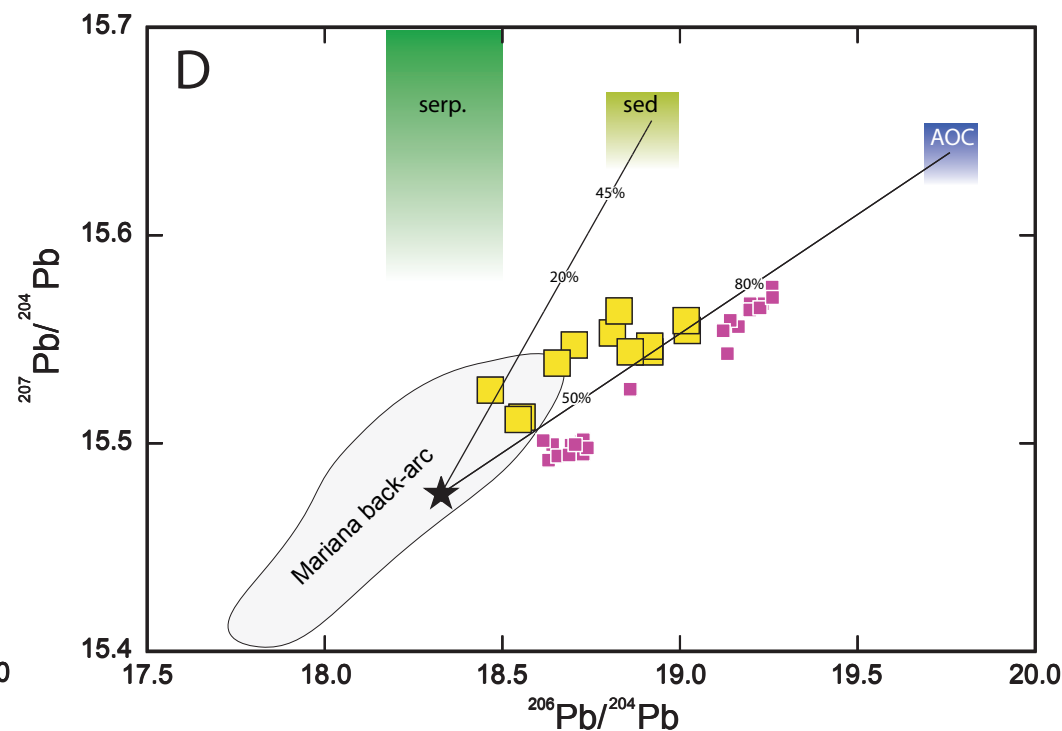
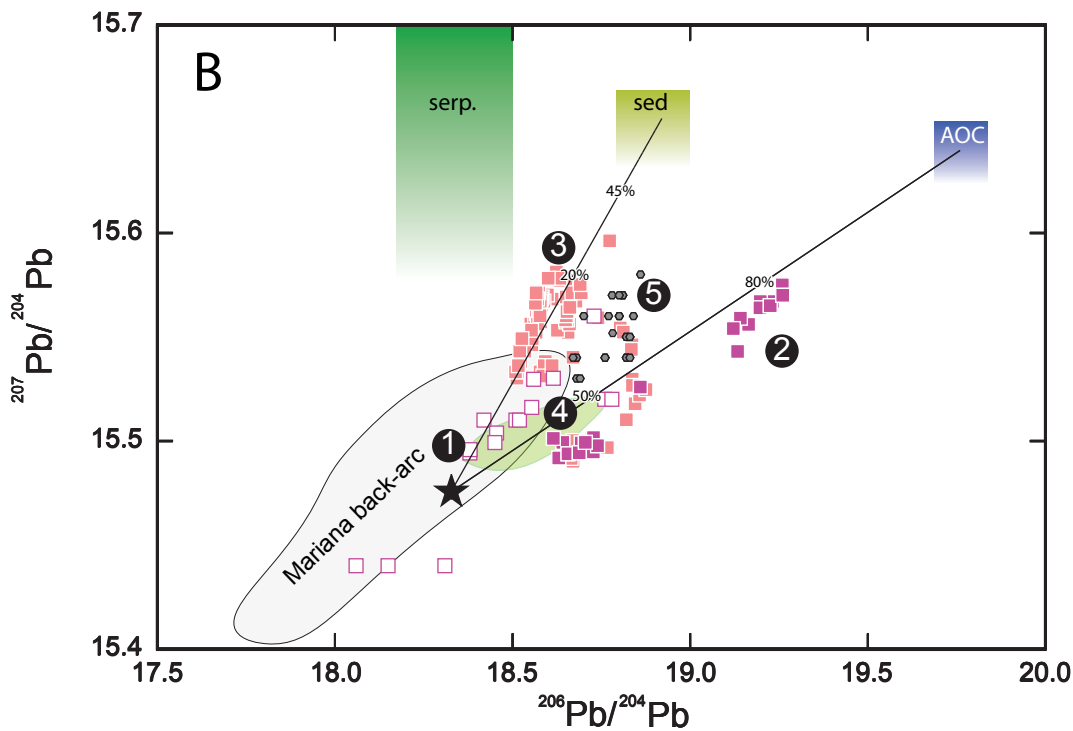
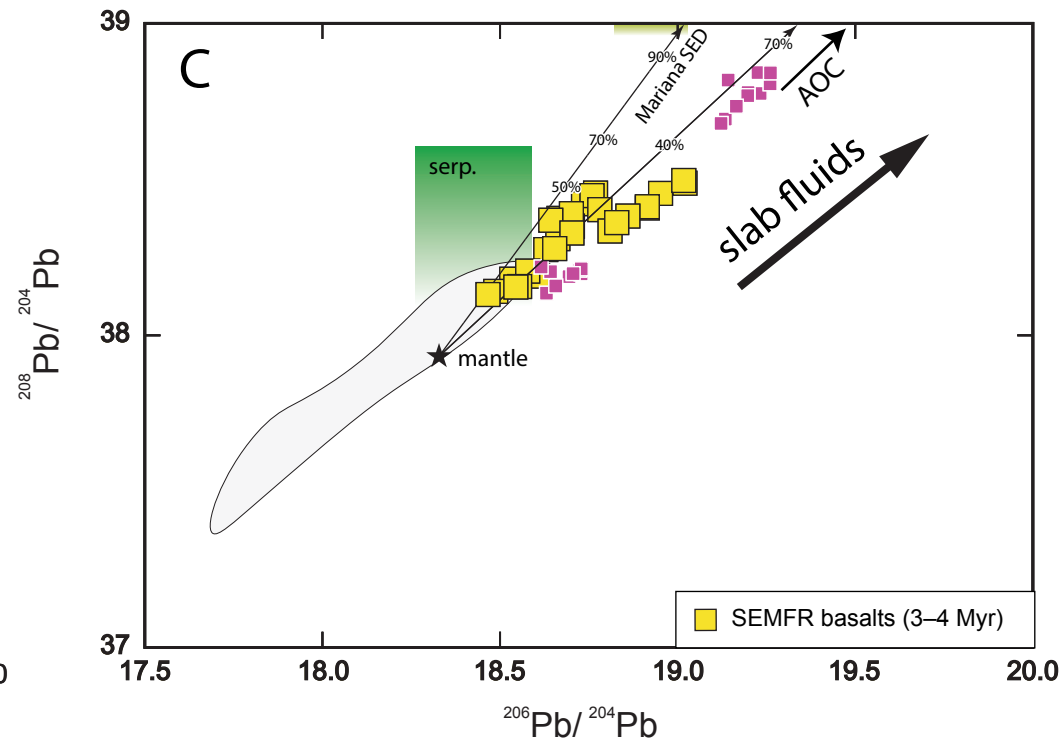
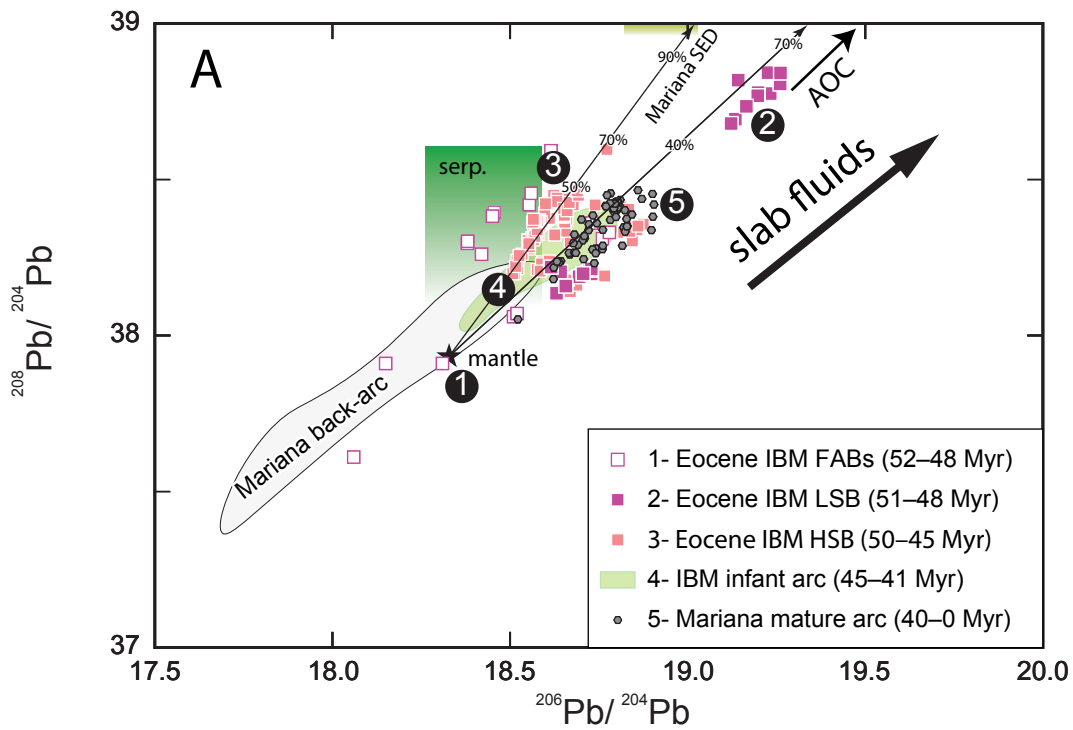
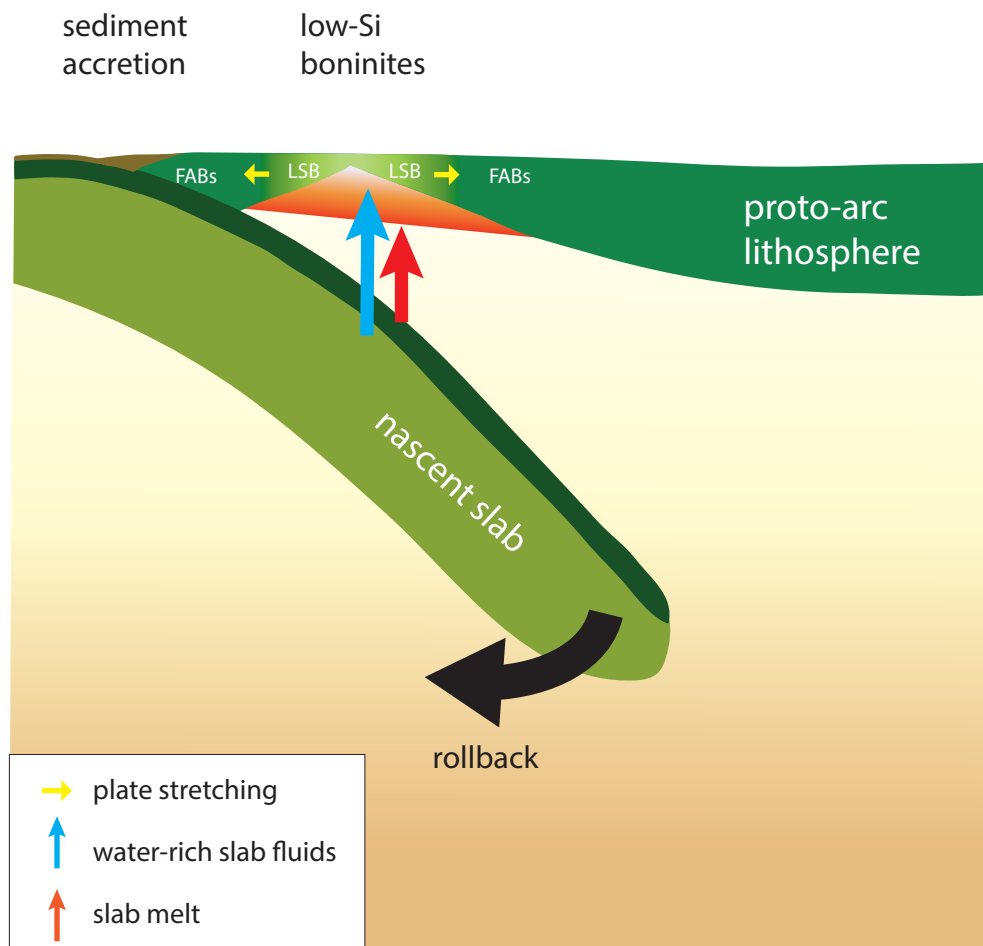


Fig. 8

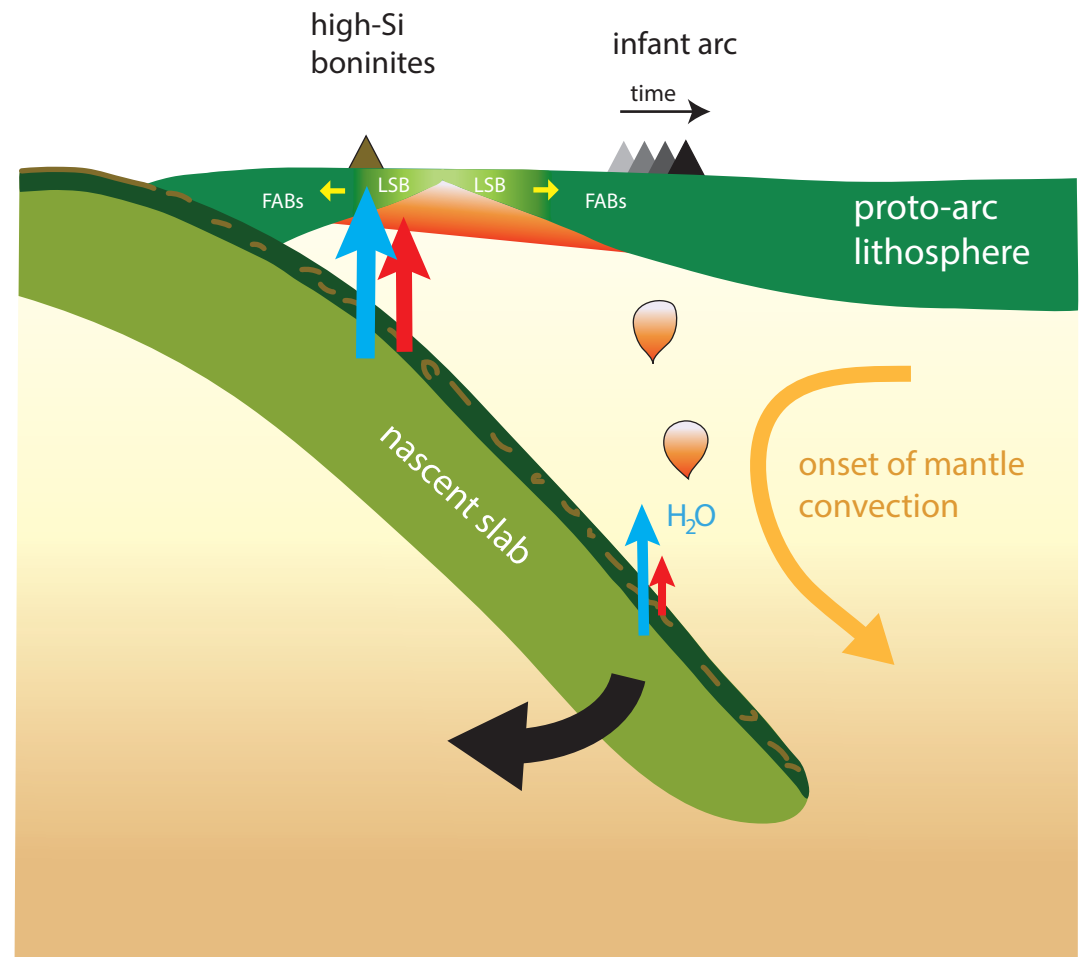




A- Formation of the proto-arc crust in IBM



B- Arc infancy



B- Mature intra-oceanic arc

